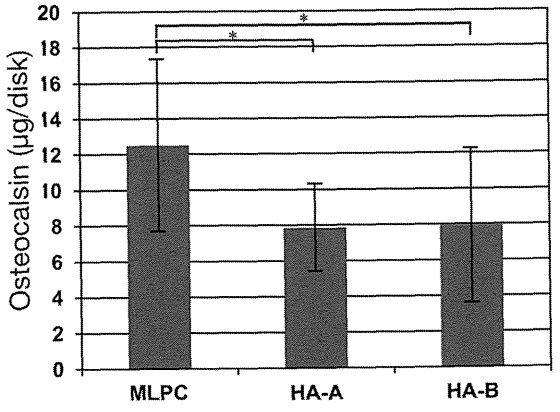

FIGURE 7. Quantification of osteocalcin content *in vivo*. Values are means ± SD (MLPC: $n = 6$, HA-A: $n = 7$, HA-B: $n = 7$). $^{*}p < 0.05$.

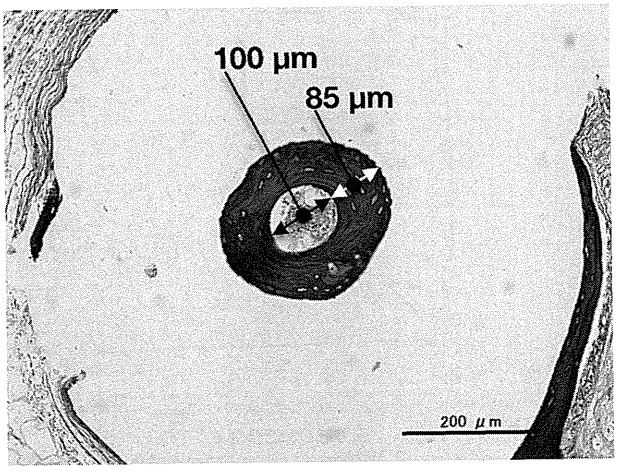

FIGURE 8. Bone formation in the through-hole that achieved homogeneously-grown new bone. [Color figure can be viewed in the online issue, which is available at wileyonlinelibrary.com.]

transfer in the porous body. Furthermore, narrow interconnecting paths decrease degassing efficiency making it more difficult to seed the porous ceramics with cells. Some porous ceramics, including HA-A and HA-B, require the application of a partial vacuum for degassing. Therefore, the width of the interconnecting paths may be more important than the pore geometries for porous implants. In our preceding study,[13] we found that pores of approximately 81 μm are likely to be filled quickly with proliferating cells, which may increase the risk of path clogging. HA-A and HA-B contain pores in this range; therefore, they would be subject to this risk. However, the clogging could potentially facilitate bone formation. This is a trade-off problem, and thus, we should recognize the importance of balancing bone formation and long-lasting fluid transfer in the pores, to the robustness of the pore-path network.

The pore shapes of MLPC are unique and clear, and they can be sorted into the following two types: through-hole on the unit and gaps among the units. The through-hole is a directly designed pore of cylindrical shape. This type can capture suspended cells efficiently by capillary action and facilitate reliable cellular aggregate formation inside the through-hole, when its diameter is properly designed. A diameter of ϕ226 μm was the optimal size for the through-hole of the HA units with respect to cellular aggregate formation, as determined in our previous study.[13] In that previous study, HA units with five types of through-hole (ϕ81, 140, 226, 310, and 441 μm) were seeded by mixing with cell suspension (MC3T3-E1, 5×10^6 cells/mL) and cultured for 1, 3, and 5 days in fresh medium to determine the optimal diameter for achieving the highest cell density in the through-hole. The through-holes in the MLPCs with cells, as expected, succeeded in achieving new bone on their inside wall. Some of the through-holes achieved homogeneous growth of new bone, which enabled us to determine the growth rate by dividing the new bone thickness by the implantation period. For example, the new bone shown in Figure 8 can be calculated to a growth rate of 2 μm/day. This growth rate calculation could be used to predict post-operative bone formation at implantation sites.

The gaps exhibit a regular construction because the spherical HA units have a strong tendency to form hexagonal closest packing arrangements in a manner similar to self-assembly. The construction can be regarded as repetitive compartments enclosed by four tetrahedrally coordinated units with four connecting paths each (Fig. 9). The connecting path is shaped like a three-pointed star edged by spherical surfaces of three HA units, and it has a width ranging from 0 (at the tangent point of the units) to $r(\sqrt{3} - 1)$ mm, where r is the radius of the HA unit and can be approximately described by an inscribed circle with a diameter of $4r(\sec 30 - 1)$ mm ($\sec 30 = 1/\cos 30$). Concerning the ϕ1 μm HA unit used in this study, the maximum widths of the gap and diameter of the inscribed circle were 730 and 310 μm, respectively. These geometries are considered to contribute to the robustness of pore network (Fig. 10). The connecting paths are wide enough to allow for fluid transfer that would feed and/or maintain cells within the pores; on the contrary, the space near the tangent point is narrow enough to facilitate rapid new bone formation, and thus the connecting paths will be reduced to the size that is conducive of new bone. This unique pore structure of MLPC gave it better osteogenic ability than HA-A and HA-B,

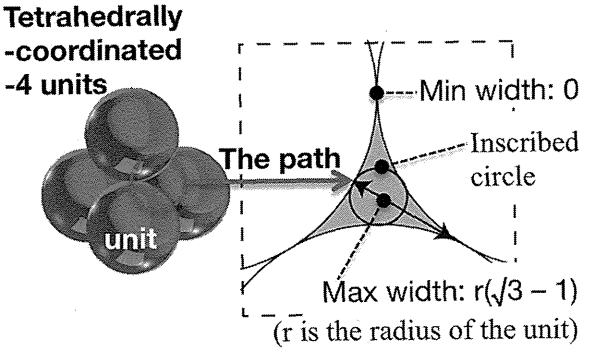

FIGURE 9. Schematic diagram of four tetrahedrally coordinated units and the connecting path. [Color figure can be viewed in the online issue, which is available at wileyonlinelibrary.com.]

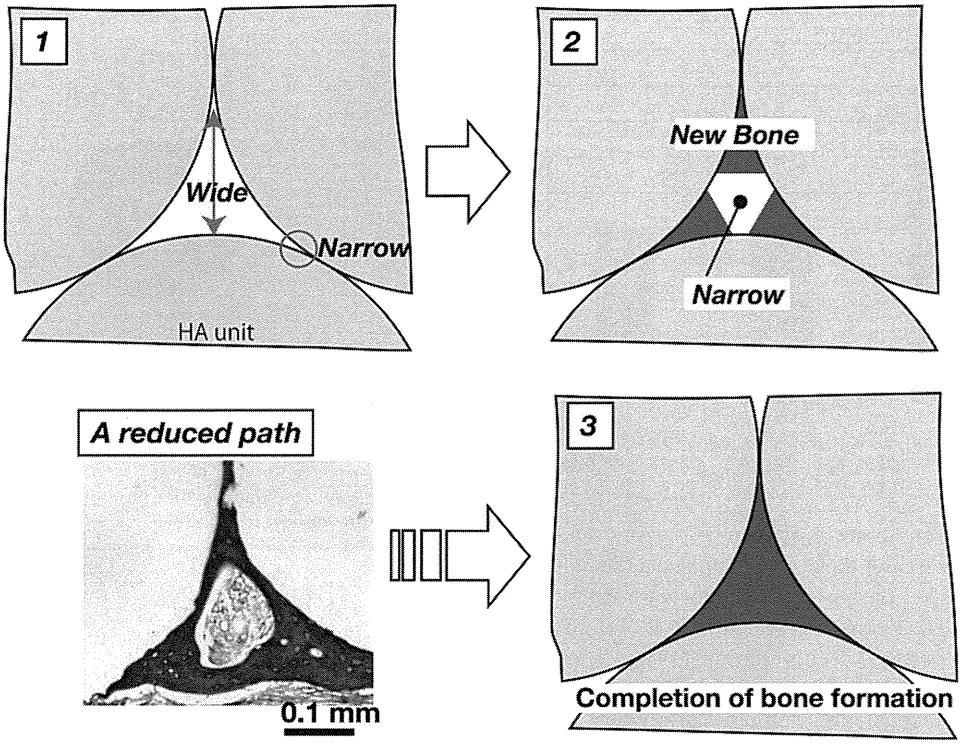

FIGURE 10. A Cascade of bone formation in the connecting path. 1. The connecting path is wide enough to allow fluid transfer, which feeds and maintains cells within the pores. The space near the tangent point is narrow enough to facilitate rapid new bone formation. 2. The volume of the connecting paths is progressively reduced via new bone formation. 3. Completion of bone formation. [Color figure can be viewed in the online issue, which is available at wileyonlinelibrary.com.]

despite the fact that the porosity of MLPC was less than that of HA-A and HA-B. Thus, bone formation in the MLPC will progress thoroughly, because of a balance of fluid transfer and bone formation in the gaps. Further, the prompt bone formation in the tangent point may function to reinforce MLPC rapidly after the implantation.

CONCLUSIONS

In this study, the MLPCs were fabricated by assembling spherical HA units with a through-hole. The through-holes functioned as fast and sure bone-forming sites, and the gaps between the spherical units formed a robust pore network that may promote bone formation and fluid transfer. As compared with commercial porous HA ceramic grafts, the osteogenic potential of MSCs on MLPC was distinguishable *in vitro* and *in vivo*, despite reduced porosity. The results suggest that the designed geometrical features of pores in the MLPC function to facilitate bone formation. And hence, the MLPC is confirmed as a capable scaffold in bone tissue engineering applications.

ACKNOWLEDGMENTS

This work was supported in part by the Ministry of Education, Culture, Sports, Science and Technology of Japan.

REFERENCES

1. Yoshikawa H, Myoui A. Bone tissue engineering with porous hydroxyapatite ceramics. J Artif Organs 2005;8:131–136.
2. Okuda K, Tai H, Tanabe K, Suzuki H, Sato T, Kawase T, Saito Y, Wolf LF, Yoshiex H. Platelet-rich plasma combined with a porous hydroxyapatite graft for the treatment of intrabony periodontal defects in humans: a comparative controlled clinical study. J Periodontol 2005;76:890–898.
3. Studart AR, Gonzenbach UT, Tervoot E, Gauckler LJ. Processing routes to macroporous ceramic: A review. J Am Ceram Soc 2006; 89:1771–1789.
4. Roy DM, Linnehan SK. Hydroxyapatite formed from coral skeletal carbonate by hydrothermal exchange. Nature 1974;247:220–222.
5. Hu J, Russell J, Ben-nissan B. Production and analysis of hydroxyapatite from Australian corals via hydrothermal process. J Mater Sci Lett 2001;20:85–87.
6. Binner JGP, Reichert J. Processing of hydroxyapatite ceramic foams. J Mater Sci 1996;31:5717–5723.
7. Sepilveda P, Binner JGP, Rogero SO, Higa OZ, Bressiani JC. Production of porous hydroxyapatite by the Gel-casting of foams and cytotoxic evaluation. J Biomed Mater Res 2000;50:27–34.
8. Hulbert SF, Morrison SJ, Klawitter JJ. Tissue reaction to three ceramics of porous and non-porous structures. J Biomed Mater Res 1972;6:347–374.
9. Karageorgiou V, Kaplan D. Porosity of 3D biomaterial scaffolds and osteogenesis. Biomaterials 2005;26:5474–5491.
10. Kuhne JH, Bartl R, Frisch B, Hammer C, Jansson V, Zimmer M. Bone formation in coralline hydroxyapatite -effects of pore size studied in rabbits. Acta Orthop Scand 1994;65:246–252.
11. Teraoka K, Yokogawa Y, Kameyama T. Construction of an interconnected pore network using hydroxyapatite beads. Key Eng Mater 2003;254:257–260.
12. Teraoka K, Yokogawa Y, Kameyama T. HA beads for bone regeneration. J Ceram Soc Jpn 2004;112:863–864.
13. Teraoka K, Saito T, Yokogawa Y. Effects of through-holes' diameter on initial cell attachment and cell proliferation. Key Eng Mater 2006;309–311:89–92.
14. Okamoto M, Dohi Y, Ohgushi H, Shimaoka H, Ikeuchi M, Matsushima A, Yonemasu K, Hosoi K. Influence of the porosity of

hydroxyapatite ceramics on in vitro and in vivo bone formation by cultured rat bone marrow stromal cells. J Mater Sci Mater Med 2006;17:327–336.

15. Tamai N, Myoui A, Tomita T, Nakase T, Tanaka J, Ochi T, Yoshikawa H. Novel hydroxyapatite ceramics with an interconnective porous structure exhibit superior osteoconduction in vivo. J Biomed Mater Res 2002;59:110–117.
16. Ito Y, Tanaka N, Fujimoto Y, Yasunaga Y, Ishida O, Agung M, Ochi M. Bone formation using novel interconnected porous calcium hydroxyapatite ceramic hybridized with cultured marrow stromal stem cells derived from Green rat. J Biomed Mater Res A 2004;69:454–461.
17. Hayashi O, Katsube Y, Hirose M, Ohgushi H, Ito H. Comparison of osteogenic ability of rat mesenchymal stem cells from bone marrow, periosteum, and adipose tissue. Calcif Tissue Int 2008;82: 238–247.
18. Tadokoro M, Hirose M, Ohgushi H. Preliminary study for evaluating bone forming ability of porous bioceramics using rat mesenchymal stem cells to be used for international standard. Key Eng Mater 2008;361–363:1161–1164.
19. Ohgushi H, Kotobuki N, Funaoka H, Machida H, Hirose M, Tanaka Y, Takakura Y. Tissue engineered ceramic artificial joint – ex vivo osteogenic differentiation of patient mesenchymal cells on total ankle joints for treatment of osteoarthritis. Biomaterials 2005;26: 4654–4661.
20. Ohgushi H, Tamai S, Dohi Y, Katuda T, Tabata S, Suwa Y. In vitro bone formation by rat marrow cell culture. J Biomed Mater Res 1996;32:333–340.
21. Nakamura A, Dohi Y, Akahane M, Ohgushi H, Nakajima H, Funaoka H, Takakura Y. Osteocalcin secretion as an early marker of in vitro osteogenic differentiation of rat mesenchymal stem cells. Tissue Eng Part C Methods 2009;15:169–180.
22. Nishikawa M, Myoui A, Ohgushi H, Ikeuch M, Tamai N, Yoshikawa H. Bone tissue engineering using novel interconnected porous hydroxyapatite ceramics combined with marrow mesenchymal cells: quantitative and three-dimensional image analysis. Cell Transplant 2004;13:367–376.

Biochemical and Biophysical Research Communications 438 (2013) 753–759

Contents lists available at ScienceDirect

Biochemical and Biophysical Research Communications

journal homepage: www.elsevier.com/locate/ybbrc

N-Cadherin is a prospective cell surface marker of human mesenchymal stem cells that have high ability for cardiomyocyte differentiation

Hisako Ishimine [a,b], Norio Yamakawa [a], Mari Sasao [c], Mika Tadokoro [c], Daisuke Kami [d], Shinji Komazaki [e], Makoto Tokuhara [f], Hitomi Takada [a], Yoshimasa Ito [a], Shinichiro Kuno [g], Kotaro Yoshimura [g], Akihiro Umezawa [d], Hajime Ohgushi [c], Makoto Asashima [a,h,i,*], Akira Kurisaki [a,b,*]

[a] Research Center for Stem Cell Engineering, National Institute of Advanced Industrial Science and Technology (AIST), Tsukuba, Ibaraki, Japan
[b] Graduate School of Life and Environmental Sciences, The University of Tsukuba, Tsukuba, Ibaraki, Japan
[c] Health Research Institute, National Institute of Advanced Industrial Science and Technology (AIST), Amagasaki, Hyogo, Japan
[d] Department of Reproductive Biology and Pathology, National Research Institute for Child Health and Development, Setagaya, Tokyo, Japan
[e] Department of Anatomy, Saitama Medical School, Iruma, Saitama, Japan
[f] Department of Surgery, Research Institute National Center for Global Health and Medicine, Shinjuku, Tokyo, Japan
[g] Department of Plastic Surgery, University of Tokyo School of Medicine, Bunkyo, Tokyo, Japan
[h] Department of Life Sciences (Biology), Graduate School of Arts and Sciences, The University of Tokyo, Meguro, Tokyo, Japan
[i] Life Science Center of TARA, The University of Tsukuba, Tsukuba, Ibaraki, Japan

ARTICLE INFO

Article history:
Received 13 July 2013
Available online 27 July 2013

Keywords:
N-cadherin
Flk-1
c-Kit
Cardiomyocyte
Mesenchymal stem cells

ABSTRACT

Mesenchymal stem cells (MSCs) are among the most promising sources of stem cells for regenerative medicine. However, the range of their differentiation ability is very limited. In this study, we explored prospective cell surface markers of human MSCs that readily differentiate into cardiomyocytes. When the cardiomyogenic differentiation potential and the expression of cell surface markers involved in heart development were analyzed using various immortalized human MSC lines, the MSCs with high expression of N-cadherin showed a higher probability of differentiation into beating cardiomyocytes. The differentiated cardiomyocytes expressed terminally differentiated cardiomyocyte-specific markers such as α-actinin, cardiac troponin T, and connexin-43. A similar correlation was observed with primary human MSCs derived from bone marrow and adipose tissue. Moreover, N-cadherin-positive MSCs isolated with N-cadherin antibody-conjugated magnetic beads showed an apparently higher ability to differentiate into cardiomyocytes than the N-cadherin-negative population. Quantitative polymerase chain reaction analyses demonstrated that the N-cadherin-positive population expressed significantly elevated levels of cardiomyogenic progenitor-specific transcription factors, including *Nkx2.5*, *Hand1*, and *GATA4* mRNAs. Our results suggest that N-cadherin is a novel prospective cell surface marker of human MSCs that show a better ability for cardiomyocyte differentiation.

1. Introduction

Stem cell therapy is expected to be an alternative regenerative medicine. In addition to embryonic stem (ES) cells and induced pluripotent stem (iPS) cells, mesenchymal stem cells (MSCs) have been shown to differentiate into various cell types including osteoblasts, chondrocytes, adipocytes, neurons, skeletal muscle fibers, and cardiomyocytes *in vitro*. However, the differentiation ability of MSCs toward cardiomyocytes is still limited [1–3]. To overcome this problem, cell surface markers specific for cardiomyogenic progenitor cells could be used to enrich better population for regenerative medicine of heart failure.

Flk-1, a vascular endothelial growth factor receptor (VEGFR2), has been reported to be a prospective cell surface marker of cardiomyocyte progenitor cells during heart development [4,5]. Flk-1 is expressed in the progenitors of multiple mesodermal lineages, including cardiac, endothelial, and vascular smooth muscle cells [5]. c-Kit (CD117) is a transmembrane tyrosine kinase receptor for Stem cell factor, and used as a cell surface marker for hematopoietic progenitors, melanocytes, mast cells, and spermatogonial stem cells. Recent research has suggested that c-Kit could be a putative cell surface marker for cardiomyogenic progenitor cells in the neonatal heart [6].

A Ca^{2+}-dependent cell–cell adhesion molecule, N-cadherin, is also expressed on cardiomyocyte progenitor cells during mouse development. N-Cadherin expression is observed in the precardiac

* Corresponding authors. Address: Research Center for Stem Cell Engineering, National Institute of Advanced Industrial Science and Technology (AIST), Tsukuba AIST Central 4-1-3105, Higashi 1-1-1, Tsukuba, Ibaraki, 305-8562, Japan. Fax: +81 29 861 2987.
E-mail addresses: asashi@bio.c.u-tokyo.ac.jp (M. Asashima), akikuri@hotmail.com (A. Kurisaki).

0006-291X/$ - see front matter © 2013 Elsevier Inc. All rights reserved.
http://dx.doi.org/10.1016/j.bbrc.2013.07.081

mesoderm at E8.5 in mice and continues to be expressed in the whole heart during development. N-Cadherin-knockout mice died by E10 because of defects in the primitive heart. Although myocardial tissue was initially formed in the knockout mouse embryos, the myocytes were subsequently dissociated, and the heart tube failed to develop [7].

In this study, we explored cell surface markers of human MSCs that have a high ability to differentiate into cardiomyocytes. We show that N-cadherin is a prospective cell surface marker of MSCs with high cardiomyogenic potential.

2. Materials and methods

2.1. Cell culture

Human MSC cell lines, UE7T-13, UE6E7T-11, UBE6T-15, UE6E7T-12, UE7T-9, and UE6E7T-2, were obtained from the JCRB Cell Bank (Osaka, Japan). They were immortalized by retrovirus gene transfer of a combination of *bmi-1*, *E6*, *E7*, and/or *hTERT* genes to human bone marrow stromal cells harvested from a 91-year-old woman [8,10]. The EPC-214 cell line was similarly immortalized at the National Research Institute for Child Health and Development (NRICHD), Japan [9]. These cell lines were maintained in DMEM high glucose (Wako) supplemented with 10% fetal calf serum (FCS; Roche). As for the primary MSCs, ANP0425 and 0607NC, were obtained from Dr. Ohgushi (National Institute of Advanced Industrial Science and Technology, Japan). MSC-R36_2 cells, MSC-R36_3 cells, and Yub623 cells were obtained from the RIKEN BRC Cell Bank (Ibaraki, Japan). Primary MSCs derived from adipose tissue (ASCs), including 09-036 (36) cells, 10-008 (8) cells, 05-055 (55) cells, and 05-076 (76) cells, were prepared at the University of Tokyo, School of Medicine Tokyo, Japan. KN-SC (KN) cells, MY-SC (MY) cells, and NN-SC (NN) cells were prepared at the Research Institute National Center for Global Health and Medicine (NCGM), Japan. Other ASCs were purchased from Invitrogen. For the ASCs, all samples except KN-SC were obtained from women aged 22–45 years (KN-SC was derived from a 41-year-old man). All of these primary cells were maintained in MesenPRO RS Basal Medium supplemented with MesenPRO RS Growth Supplement (GIBCO). Cells were maintained in a humidified incubator at 37 °C with an atmosphere of 5% CO_2. All the experiments using human materials were approved by the Human Ethics Committee at AIST, NRICHD, NCGM, and the University of Tokyo. Human umbilical vein endothelial cells (HUVEC) were cultured in RPMI-1640 supplemented with EGM-2 SingleQuots (LONZA) and penicillin/streptomycin (Wako). TF-1 cells were cultured in RPMI-1640 supplemented with 10% FBS, 2 ng/mL rhGM-CSF, and penicillin/streptomycin (Wako).

2.2. Preparation of mouse fetal cardiomyocytes

The fetal hearts of E16.5 ICR mice were cut into small pieces and washed with phosphate-buffered saline (PBS). They were incubated with 0.15% trypsin and 0.012% EDTA in PBS at 37 °C for 10 min under gentle stirring. The supernatant containing the dissociated cardiomyocytes was mixed with DMEM supplemented with 10% FCS, and centrifuged at 1000 rpm for 5 min. The pellet was then re-suspended in 10 mL of DMEM with 10% FCS and incubated on a glass dish for 1 h to remove fibroblasts. The floating cardiomyocytes were collected and re-plated at $5 \times 10^5/cm^2$ on gelatin-coated glass bottom dishes (Asahi Techno Glass). All the experiments using animals were approved by the Animal Experiment Committee at AIST.

2.3. Immunoblotting analysis

Human MSC cell lines were homogenized in a lysis buffer containing 20 mM Tris–HCl (pH 7.4), 300 mM NaCl, 0.5 mM EDTA, 1% NP-40, and a complete protease inhibitor cocktail (Roche). After centrifugation at 13,000 rpm for 10 min at 4 °C, equal protein amounts were separated by SDS–PAGE (5–20%). The blots were incubated with antibodies against N-cadherin (1:200; C3865, Sigma), Flk-1 (1:100, 10347; IBL), c-Kit (1:200, AF332; R&D Systems), Integrin-α4 (1:200; sc-14008, Santa Cruz), VCAM-1 (1:200; sc-8304, Santa Cruz), PDGFRα (1:200; 323503, BioLegend), Nkx2.5 (1:200; sc-14033, Santa Cruz), GATA4 (1:200; sc-9053, Santa Cruz), or β-tubulin (1:1000, RB-9249; NeoMarkers). Proteins were detected with an enhanced chemiluminescence (ECL) reagent (Super-Signal West Femto Maximum Sensitivity Substrate, Pierce) using an LAS-3000 Image Analyzer (Fuji Film).

2.4. Flow cytometry analysis

All MSCs were harvested with cell dissociation buffer (GIBCO) and blocked with normal sheep IgG on ice for 1 h. Cells were incubated with biotinylated anti-N-cadherin antibody (1:100, BAF1388; R&D System), anti-Flk-1 antibody (1:100, 10347; IBL), and APC-conjugated anti-c-Kit antibody (1:100, 550412; Becton Dickinson) on ice for 1 h. The N-cadherin antibody was fluorescently labeled using Allophycocyanin-Alexa Fluor 750 streptavidin (Molecular Probes). The Flk-1 antibody was fluorescently labeled with the Alexa Fluor 488-conjugated secondary antibody (Molecular Probes). Cells were resuspended in buffer with propidium iodide (Sigma). Analysis was performed with a FACS Aria (Becton Dickinson) and FlowJo software (TOMY Digital Biology) with propidium iodide-negative population. The data were obtained from at least two independent experiments.

3. Results

MSCs are a mixture of primary adherent cells derived from the stroma of adult tissues. The multipotency of MSCs rapidly decreases as the passage number increases. Therefore, it is not easy to obtain reproducible data from these heterogeneous primary cells. To overcome these problems, we took advantage of immortalized human MSC clones with *bmi-1*, *TERT*, *E6*, and/or *E7*, which retain their multipotent differentiation ability over a long time when cultured *in vitro* [8].

Cardiac differentiation of human MSCs was performed by co-culturing with mouse fetal cardiomyocytes, which is a well-established method to differentiate MSCs into electro-physiologically validated cardiomyocytes [9,10]. Human MSC cell lines were labeled with a GFP-expressing lentivirus and then cultured on a cardiomyocyte feeder cells prepared from mouse embryonic heart tissue (Fig. S1A). On day 7, human MSC lines such as EPC-214 and UE7T-13 differentiated into cardiomyocytes. Around 5% of these GFP-labeled MSCs differentiated into beating cardiomyocytes (Fig. 1A). GFP-positive, differentiated cardiomyocytes showed autonomously periodical contractions (Fig. S1B). Significant number of GFP-positive human MSCs expressed cardiomyocyte-specific terminal differentiation markers (Fig. S1C, left and middle, Fig. S1D, left, and a confocal image Fig. S1E). On the other hand, some cell lines did not differentiate into beating cardiomyocytes under identical conditions (UE7T-9, UE6E7T-2) (Fig. S1C right and Fig. S1D right).

Next, the efficiency of human MSCs differentiation into spontaneously beating cardiomyocytes was quantified by counting the number of GFP-positive and spontaneously beating cardiomyocytes with a fluorescence microscope on day 7 (Fig. 1A). The

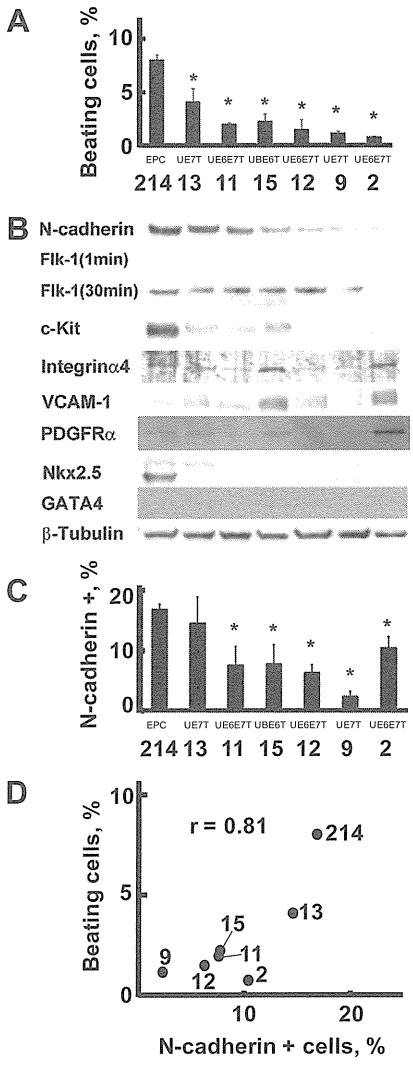

Fig. 1. Correlation between cardiomyogenic differentiation efficiency and cell surface protein marker expression in human MSC cell lines. (A) Autonomously beating cardiomyocytes differentiated from GFP-labeled human MSC lines, EPC-214, UE7T-13, UE6E7T-11, UBE6T-15, UE6E7T-12, UE7T-9, and UE6E7T-2, were counted under a fluorescence microscope. (B) The expression of cell surface proteins and transcription factors related to cardiovascular development were analyzed by immunoblotting of whole cell lysates. (C) Flow cytometric analysis of cell surface expression of N-cadherin in human MSC lines. (D) Correlation between the differentiation efficiency into cardiomyocytes and cell surface N-cadherin expression in human MSC lines. The vertical axis represents the differentiation efficiency. The horizontal axis represents cell surface expression of N-cadherin. The correlation coefficient (r) is shown on the graph. $^*P < 0.05$.

expression of various cell surface proteins, which are essential for the development of the heart *in vivo* or are specifically expressed in cardiovascular progenitor cells, was examined by immunoblotting (Fig. 1B). Among these markers, the expression of N-cadherin showed a good correlation with the differentiation efficiency toward beating cardiomyocytes. The MSC lines highly expressing N-cadherin showed higher differentiation ability toward cardiomyocytes. Flk-1 also showed an expression pattern similar to that of N-cadherin. However, the expression levels in human MSCs were very low. Only an extremely long exposure (30 min) enabled us to detect the Flk-1 protein bands (Fig. 1B). The expression of c-Kit showed some correlation with the cardiomyogenic differentiation abilities of these cells, although the expression levels of c-Kit in some human MSCs that readily differentiated into cardiomyocytes were very low (Fig. 1B, UE7T-13, UE6E7T-11, and UBE6T-15).

Other cell surface proteins have been reported as essential for heart development. Integrin α4 is essential for the development of the heart and placenta [11]; a homozygous null mutant of integrin α4 caused embryonic lethality due to defects in the epicardium and coronary vessel development, leading to cardiac hemorrhage, in addition to failure of fusion between the allantois and chorion during placentation. Knockout mice of vascular cell adhesion molecule 1 (VCAM-1) displayed a reduction in the compact layer of the ventricular myocardium and intraventricular septum [12]. Platelet-derived growth factor receptor α (Pdgfrα) is expressed in cardiac progenitor cells in the posterior part of the secondary heart field. Pdgfrα is also expressed in the valves and pericardia of the heart at E12.5–16.5 [13]. However, the expression of these cell surface proteins did not show a strong correlation with the differentiation ability of human MSCs into cardiomyocytes (Fig. 1A and B).

Next, we verified the cell surface-specific expression of N-cadherin, Flk-1, and c-Kit in living MSCs by flow cytometry. Flk-1 was barely detectable on the cell surface of human MSCs (Fig. 2A), although a positive control, HUVEC, showed strong cell surface expression of Flk-1 (Fig. 2A, right), indicating that human MSCs do not express detectable amounts of Flk-1 on the plasma membrane. The cell surface expression of c-Kit was also relatively low (Fig. 2B), and the MSC lines with higher differentiation ability toward cardiomyocytes did not show a significant amount of cell surface expression of c-Kit (Fig. 2B, UE7T-13).

By contrast, N-cadherin was readily detectable in the human MSC lines with high differentiation ability toward beating cardiomyocytes (Fig. 2C). When the cell surface expression of N-cadherin (Fig. 1C) and the differentiation ability into beating cardiomyocytes (Fig. 1A) were compared with human MSC cell lines, a strong correlation was observed between these 2 events ($r = 0.81$; Fig. 1D). Immunofluorescence analysis of the human MSC line EPC-214, which readily differentiated into cardiomyocytes, showed characteristic localization of N-cadherin in cell-to-cell contacts in addition to the uniform expression on the plasma membrane (Fig. 2D). However, UE7T-9 cells, which expressed N-cadherin at low levels and did not differentiate into cardiomyocytes, did not show significant expression of N-cadherin (Fig. 2D, right). These results suggest that N-cadherin could be a good prospective cell surface marker of cardiomyogenic human MSCs.

Next, we validated the expression of N-cadherin with various primary human MSCs. Human bone marrow-derives MSCs (BMSCs) cultured for a limited number of passages gave a good correlation between the cell surface expression of N-cadherin and the differentiation ability into beating cardiomyocytes (Fig. 3A and B). Human MSCs derived from adipose tissue (ASCs) also showed similar results (Fig. 3D and E). The Pearson's correlation coefficients of cell surface expression of N-cadherin and differentiation efficiency toward beating cardiomyocytes in BMSCs and ASCs were good in both cases (0.55 and 0.77, respectively; Fig. 3C and F). As for c-Kit, we failed to detect significant expression of c-Kit in primary MSCs that showed distinct cardiomyogenic differentiation abilities (Fig. S2, 36_2). c-Kit protein could be detected on the cell surface of some primary ASCs (Fig. S2B, 1212). However, the isolation of c-Kit-positive cells from these primary ASCs was not successful by flow cytometry.

To determine whether the N-cadherin-positive population of human MSCs has higher differentiation ability into cardiomyocytes than N-cadherin-negative MSCs, we established the separation conditions of N-cadherin-positive cells using MACS (Fig. S3). Then, the N-cadherin-positive fraction was concentrated from a primary culture of human ASCs (1212 used in Fig. 3) using the same method (Fig. 4A); these cells were further cultured on mouse embryonic heart feeder cells for 7 days. The enriched ASC fraction expressing cell surface N-cadherin showed a 4-fold higher cardiomyogenic differentiation ability than the N-cadherin-negative fraction (Fig. 4B).

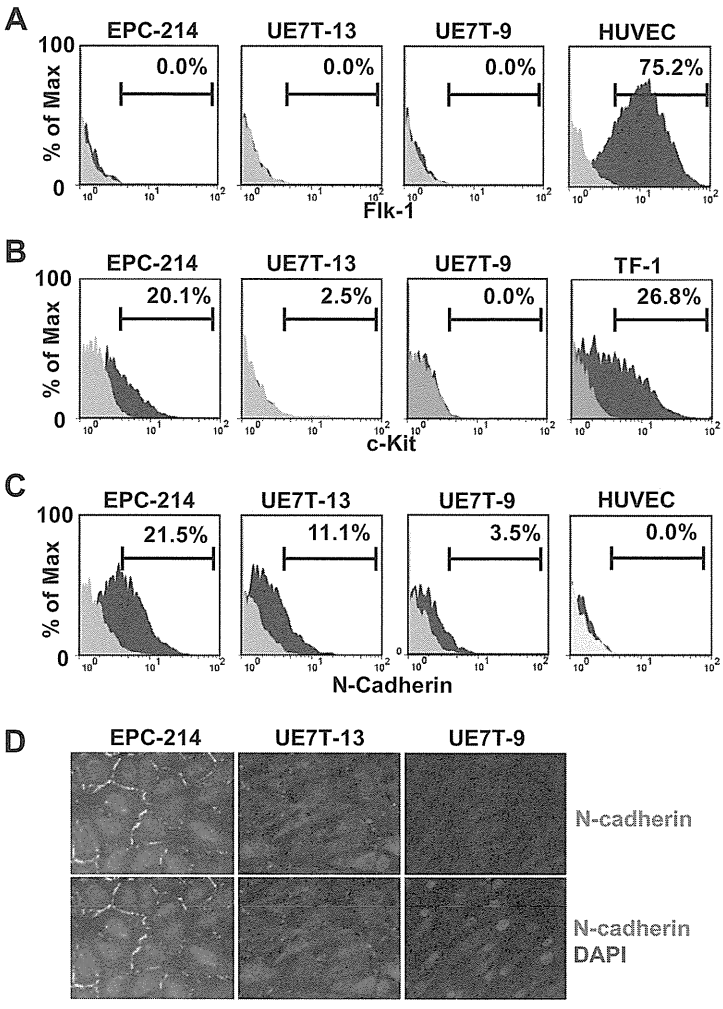

Fig. 2. Representative FACS plots of cell surface protein expression in human MSC cell lines. The live cells were immunostained with (A) Flk-1, (B) c-Kit, or (C) N-cadherin antibodies. Propidium iodide-positive cells were excluded from the analysis. (D) Localization of N-cadherin in human MSCs. The indicated human MSC lines were immunostained with N-cadherin antibody (green) and DAPI (blue). (For interpretation of the references to colour in this figure legend, the reader is referred to the web version of this article.)

To characterize the cardiomyogenic N-cadherin-positive population, we analyzed the gene expression profiles of the MACS-sorted fractions with microarray. Gene ontology analysis of 3056 genes (among 44,000 genes) that exhibited more than a 1.5-fold difference identified molecular functions associated with zinc ion binding, transition metal ion binding, and nucleic acid binding (Fig. S4A) and biological functions involved in DNA binding, gene expression, transcription, and metabolic processes of nucleic acid (Fig. S4B). These results suggested that N-cadherin-positive cells showed higher expression of specific DNA-binding proteins and elevated metabolic activity. On the other hand, the N-cadherin-negative population showed higher expression of genes involved in the MHC class I protein complex, vacuole organization, and GTPase activity (Fig. S4C and S4D).

When the expression of various lineage marker genes was compared, the N-cadherin-positive fraction showed up-regulated expression of genes involved in the differentiation of cardiomyocytes and skeletal myocytes, such as *Nkx2.5*, *Hand1*, *Tnni3* (*cTnI*), and *Myog* (Fig. 4C). In contrast, ectodermal and endodermal lineage markers were the same among the MACS-sorted fractions, with the exception of *Pax4*, a transcription factor involved in pancreatic development. Although MSCs efficiently differentiate into osteoblasts, chondrocytes, and adipocytes, these specific markers did not show a large difference. The expression of MSC-specific cell surface markers was not increased in the N-cadherin-positive fraction.

Quantitative PCR analysis revealed significant up-regulation of a cardiomyogenic precursor-specific gene, *Nkx2.5*, in the N-cadherin-positive fraction, for more than 200-times higher than that in the N-cadherin-negative fraction. Two other transcription factors, *Hand1* and *Gata4*, but not Tbx5, also showed significantly elevated expression in the N-cadherin-positive fraction (Fig. 4D). Interestingly, the expression of *Myog*, a transcription factor involved in skeletal muscle development, was also elevated in the N-cadherin-positive fraction. Although terminal markers for cardiomyocytes, such as *Anp* and *cTnI*, showed higher expression in the N-cadherin-positive fraction (Fig. 4E), the expression levels of these terminal markers were very low, suggesting that N-cadherin-positive cells may be ready for differentiation, but not terminally differentiated into cardiomyocytes.

Interestingly, the expression of some pluripotency-specific genes such as *Oct4* (*Pou5f1*), *Sall4*, and *Nanog* was significantly up-regulated in the N-cadherin-positive population (Fig. 4F and G). However, these expression in human MSCs was not as high as that in human ES cells (Fig. 4F), suggesting that these genes up-regulated in N-cadherin-positive MSCs may not exhibit pluripotency as observed in ES/iPS cells.

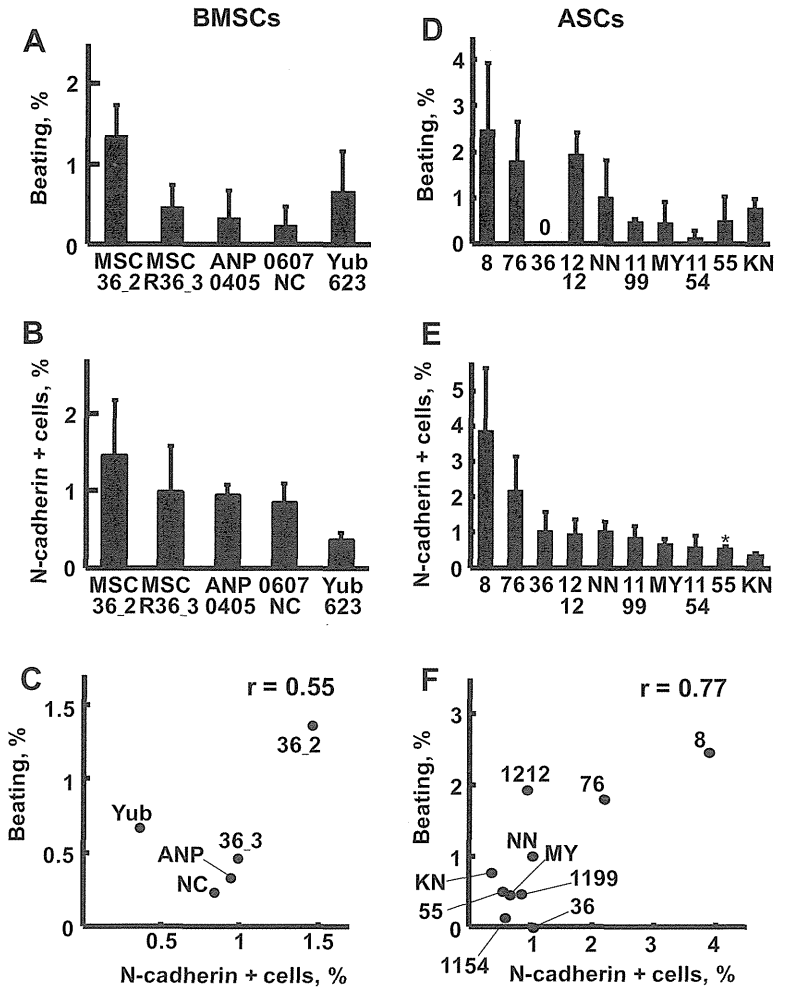

Fig. 3. Differentiation efficiency of primary human MSCs into cardiomyocytes and cell surface expression of N-cadherin. In this experiment, primary human MSCs derived from (A–C) the bone marrow (BMSCs) or (D–F) adipose-derived tissue (ASCs) were used. (A, D) Differentiation efficiency of primary human MSCs into cardiomyocytes. Autonomously beating cardiomyocytes differentiated from GFP-labeled human (A) BMSCs or (D) ASCs were counted using a microscope. (B, E) Flow cytometric analysis of cell surface expression of N-cadherin in primary human (B) BMSCs or (E) ASCs. *$P < 0.05$. (C, F) Correlation between the differentiation efficiency into beating cardiomyocytes and the cell surface N-cadherin expression of primary human (C) BMSCs or (F) ASCs. The correlation coefficient (r) is shown on the graph.

4. Discussion

In this study, we have identified N-cadherin as a reliable cell surface marker for human MSCs with higher differentiation ability toward cardiomyocytes. N-cadherin is continuously expressed from cardiomyogenic progenitor cells to mature cardiomyocytes in the adult heart. N-cadherin maintains the functional gap junction complex at the plasma membrane in the adult heart, and conditional knockout of N-cadherin in mice resulted in arrhythmia in adult hearts with significant decreases in Cn43 and Cn40 [17].

We have previously shown that the cardiomyogenic progenitor cells differentiated from mouse ES cells expressed high levels of N-cadherin on the cell surface membrane, and an antibody against N-cadherin could be used to concentrate the progenitor cells from a heterogeneous cell population differentiated from mouse ES cells [18]. Although the possible differentiation pathway of cardiomyocytes from pluripotent ES cells and multipotent MSCs may not be the same, N-cadherin could be a common progenitor marker of the cardiomyogenic cells derived from these stem cells.

In addition to cardiomyogenic genes, we observed increased expression of pluripotency-specific transcription factors of ES cells, such as *Oct4*, *Sall4*, and *Nanog*, in the N-cadherin-positive fraction. Recently, *Oct4* has been suggested to be the gatekeeper into and out of the reprogramming expressway [19]. Therefore, the elevated expression of *Oct4* and related transcription factors could positively modulate the differentiation ability of MSCs. For example, overexpression of the *Oct4* gene enhanced the differentiation ability of MSCs [14], and knockdown of *Oct4* caused loss of multiple differentiation potential [15]. Nanog was also shown to possess similar activity in BMSCs [16]. Therefore, N-cadherin-positive cells with up-regulated expression of *Oct4* and other transcription factors responsible for cardiomyogenesis may increase the differentiation ability of MSCs into cardiomyocytes.

N-Cadherin is localized in the cell–cell contacts of cardiomyocytes and plays essential roles for formation of the cardiac intercalated disk structure that electromechanically couples adjacent cardiac myocytes. Addition of antibodies against N-cadherin to the cultured cardiomyocytes [20], mesodermal explants [21] or injected into embryos [22] caused a reduction in the number of myofibrils and destroy stress fibers [23]. In primary cardiomyocytes dissociated from adult rat heart, N-cadherin diffusely distributed around the cell periphery begins to co-localize with desmocollin, plakoglobin, and plakophilin-2 at the cell contact sites. The newly generated adhesive contacts sequentially recruit desmoplakin, intermediate filaments, connexin-43, and ankyrin-G. Subsequently, the voltage-gated sodium channel is incorporated into mature intercalated disks. This assembly process requires the clustering of transmembrane adhesive contacts with N-cadherin

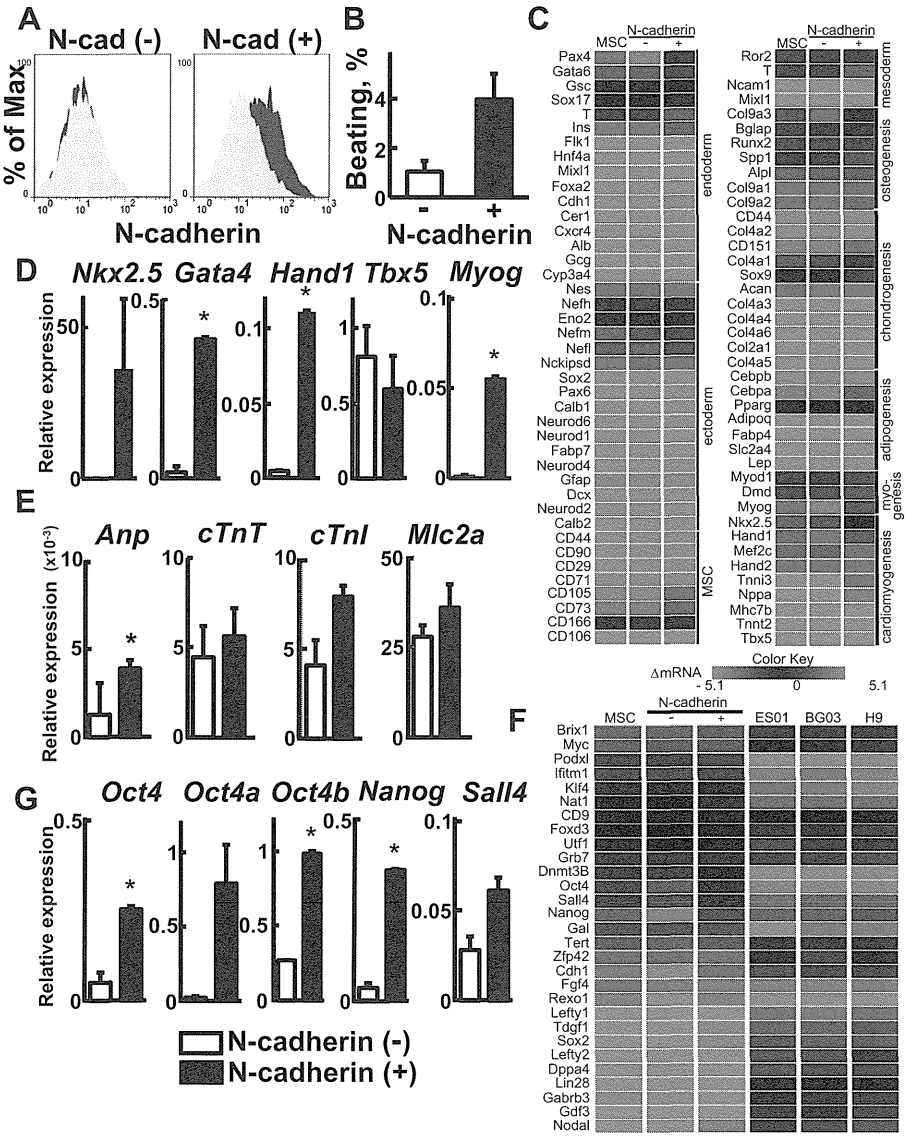

Fig. 4. Separation of N-cadherin-positive cells from the primary MSCs derived from adipose tissue (1212) with anti-N-cadherin antibody-conjugated magnetic beads. (A) The FACS histograms represent cell surface N-cadherin expression in the N-cadherin-negative fraction (left) and N-cadherin-positive fraction (right). (B) Differentiation efficiency of the purified primary ASCs into beating cardiomyocytes. Bar graphs represent the mean value of differentiation efficiency obtained from two independent experiments. (C) Heat map profile of lineage-specific differentiation marker expression in ASCs. The N-cadherin-positive fraction showed elevated expression of specific genes involved in cardiomyogenesis. (D, E) qPCR analysis of cardiomyogenic progenitor-specific transcription factors (D) and terminal differentiation markers for heart development (E). (F) Heat map profile of pluripotency-specific marker expression in human ASCs and human ES cells (ES01, BG03, and H9). (G) qPCR analysis of the expression of pluripotency-specific transcription factors in MACS-sorted fractions. $^{*}P < 0.05$. (For interpretation of the references to colour in (C) and (F), the reader is referred to the web version of this article.)

[24]. Therefore, MSCs with higher expression of N-cadherin may have preferable potential for the differentiation into cardiomyocytes. N-cadherin is expressed in pericytes and is involved in the interaction between pericytes and endothelial cells during vessel formation *in vivo* [25,26]. Pericytes in MSCs could be one of the possible cell sources that show higher differentiation ability toward cardiomyocytes.

Disclosure statement

No competing financial interests exist.

Acknowledgments

We would like to thank to Dr. Yuzuru Ito for discussion. The lentiviral vector for GFP was provided by Dr. Miyoshi (Riken BRC) through the National Bio-Resource Project of the MEXT, Japan. This research was supported by NEDO of Japan (New Energy and Industrial Development Organization, Translational Research Promotion Project).

Appendix A. Supplementary data

Supplementary data associated with this article can be found, in the online version, at http://dx.doi.org/10.1016/j.bbrc.2013.07.081.

References

[1] M. Shiota, T. Heike, M. Haruyama, S. Baba, A. Tsuchiya, H. Fujino, H. Kobayashi, T. Kato, K. Umeda, M. Yoshimoto, T. Nakahata, Isolation and characterization of bone marrow-derived mesenchymal progenitor cells with myogenic and neuronal properties, Exp. Cell Res. 313 (2007) 1008–1023.
[2] S. Wakitani, T. Saito, A.I. Caplan, Myogenic cells derived from rat bone marrow mesenchymal stem cells exposed to 5-azacytidine, Muscle Nerve 18 (1995) 1417–1426.

[3] S. Makino, K. Fukuda, S. Miyoshi, F. Konishi, H. Kodama, J. Pan, M. Sano, T. Takahashi, S. Hori, H. Abe, J. Hata, A. Umezawa, S. Ogawa, Cardiomyocytes can be generated from marrow stromal cells in vitro, J. Clin. Invest. 103 (1999) 697–705.
[4] J.K. Yamashita, M. Takano, M. Hiraoka-Kanie, C. Shimazu, Y. Peishi, K. Yanagi, A. Nakano, E. Inoue, F. Kita, S. Nishikawa, Prospective identification of cardiac progenitors by a novel single cell-based cardiomyocyte induction, FASEB J. 19 (2005) 1534–1536.
[5] S.J. Kattman, T.L. Huber, G.M. Keller, Multipotent flk-1+ cardiovascular progenitor cells give rise to the cardiomyocyte, endothelial, and vascular smooth muscle lineages, Dev. Cell 11 (2006) 723–732.
[6] Y.N. Tallini, K.S. Greene, M. Craven, A. Spealman, M. Breitbach, J. Smith, P.J. Fisher, M. Steffey, M. Hesse, R.M. Doran, A. Woods, B. Singh, A. Yen, B.K. Fleischmann, M.I. Kotlikoff, C-kit expression identifies cardiovascular precursors in the neonatal heart, Proc. Natl. Acad. Sci. USA 106 (2009) 1808–1813.
[7] G.L. Radice, H. Rayburn, H. Matsunami, K.A. Knudsen, M. Takeichi, R.O. Hynes, Developmental defects in mouse embryos lacking N-cadherin, Dev. Biol. 181 (1997) 64–78.
[8] T. Mori, T. Kiyono, H. Imabayashi, Y. Takeda, K. Tsuchiya, S. Miyoshi, H. Makino, K. Matsumoto, H. Saito, S. Ogawa, M. Sakamoto, J. Hata, A. Umezawa, Combination of hTERT and bmi-1, E6, or E7 induces prolongation of the life span of bone marrow stromal cells from an elderly donor without affecting their neurogenic potential, Mol. Cell. Biol. 25 (2005) 5183–5195.
[9] K. Okamoto, S. Miyoshi, M. Toyoda, N. Hida, Y. Ikegami, H. Makino, N. Nishiyama, H. Tsuji, C.H. Cui, K. Segawa, T. Uyama, D. Kami, K. Miyado, H. Asada, K. Matsumoto, H. Saito, Y. Yoshimura, S. Ogawa, R. Aeba, R. Yozu, A. Umezawa, 'Working' cardiomyocytes exhibiting plateau action potentials from human placenta-derived extraembryonic mesodermal cells, Exp. Cell Res. 313 (2007) 2550–2562.
[10] Y. Takeda, T. Mori, H. Imabayashi, T. Kiyono, S. Gojo, S. Miyoshi, N. Hida, M. Ita, K. Segawa, S. Ogawa, M. Sakamoto, S. Nakamura, A. Umezawa, Can the life span of human marrow stromal cells be prolonged by bmi-1, E6, E7, and/or telomerase without affecting cardiomyogenic differentiation?, J Gene Med. 6 (2004) 833–845.
[11] J.T. Yang, H. Rayburn, R.O. Hynes, Cell adhesion events mediated by alpha 4 integrins are essential in placental and cardiac development, Development 121 (1995) 549–560.
[12] L. Kwee, H.S. Baldwin, H.M. Shen, C.L. Stewart, C. Buck, C.A. Buck, M.A. Labow, Defective development of the embryonic and extraembryonic circulatory systems in vascular cell adhesion molecule (VCAM-1) deficient mice, Development 121 (1995) 489–503.
[13] N. Takakura, H. Yoshida, Y. Ogura, H. Kataoka, S. Nishikawa, PDGFR alpha expression during mouse embryogenesis: immunolocalization analyzed by whole-mount immunohistostaining using the monoclonal anti-mouse PDGFR alpha antibody APA5, J. Histochem. Cytochem. 45 (1997) 883–893.
[14] T.M. Liu, Y.N. Wu, X.M. Guo, J.H. Hui, E.H. Lee, B. Lim, Effects of ectopic Nanog and Oct4 overexpression on mesenchymal stem cells, Stem Cells Dev. 18 (2009) 1013–1022.
[15] C.C. Tsai, P.F. Su, Y.F. Huang, T.L. Yew, S.C. Hung, Oct4 and Nanog directly regulate Dnmt1 to maintain self-renewal and undifferentiated state in mesenchymal stem cells, Mol. Cell 47 (2012) 169–182.
[16] M.J. Go, C. Takenaka, H. Ohgushi, Forced expression of Sox2 or Nanog in human bone marrow derived mesenchymal stem cells maintains their expansion and differentiation capabilities, Exp. Cell Res. 314 (2008) 1147–1154.
[17] J. Li, V.V. Patel, I. Kostetskii, Y. Xiong, A.F. Chu, J.T. Jacobson, C. Yu, G.E. Morley, J.D. Molkentin, G.L. Radice, Cardiac-specific loss of N-cadherin leads to alteration in connexins with conduction slowing and arrhythmogenesis, Circ. Res. 97 (2005) 474–481.
[18] M. Honda, A. Kurisaki, K. Ohnuma, H. Okochi, T.S. Hamazaki, M. Asashima, N-cadherin is a useful marker for the progenitor of cardiomyocytes differentiated from mouse ES cells in serum-free condition, Biochem. Biophys. Res. Commun. 351 (2006) 877–882.
[19] J. Sterneckert, S. Hoing, H.R. Scholer, Concise review: Oct4 and more: the reprogramming expressway, Stem Cells 30 (2012) 15–21.
[20] A.P. Soler, K.A. Knudsen, N-cadherin involvement in cardiac myocyte interaction and myofibrillogenesis, Dev. Biol. 162 (1994) 9–17.
[21] K. Imanaka-Yoshida, K.A. Knudsen, K.K. Linask, N-cadherin is required for the differentiation and initial myofibrillogenesis of chick cardiomyocytes, Cell Motil. Cytoskeleton 39 (1998) 52–62.
[22] K.K. Linask, K.A. Knudsen, Y.H. Gui, N-cadherin-catenin interaction: necessary component of cardiac cell compartmentalization during early vertebrate heart development, Dev. Biol. 185 (1997) 148–164.
[23] T. Volk, B. Geiger, A-CAM: a 135-kD receptor of intercellular adherens junctions. I. Immunoelectron microscopic localization and biochemical studies, J. Cell Biol. 103 (1986) 1441–1450.
[24] S.B. Geisler, K.J. Green, L.L. Isom, S. Meshinchi, J.R. Martens, M. Delmar, M.W. Russell, Ordered assembly of the adhesive and electrochemical connections within newly formed intercalated disks in primary cultures of adult rat cardiomyocytes, J. Biomed. Biotechnol. 2010 (2010) 624719.
[25] H. Gerhardt, H. Wolburg, C. Redies, N-cadherin mediates pericytic-endothelial interaction during brain angiogenesis in the chicken, Dev. Dyn. 218 (2000) 472–479.
[26] E. Tillet, D. Vittet, O. Feraud, R. Moore, R. Kemler, P. Huber, N-cadherin deficiency impairs pericyte recruitment, and not endothelial differentiation or sprouting, in embryonic stem cell-derived angiogenesis, Exp. Cell Res. 310 (2005) 392–400.

JOURNAL OF TISSUE ENGINEERING AND REGENERATIVE MEDICINE
J Tissue Eng Regen Med 2013; 7: 51–60.
Published online 9 February 2012 in Wiley Online Library (wileyonlinelibrary.com) **DOI:** 10.1002/term.495

RESEARCH ARTICLE

Mesenchymal stromal cells improve the osteogenic capabilities of mineralized agarose gels in a rat full-thickness cranial defect model

Norihiko Mizuta[1,2], Koji Hattori[2]*, Yoshika Suzawa[1], Soichi Iwai[1], Tomohiro Matsumoto[2], Mika Tadokoro[2], Takayoshi Nakano[3], Mitsuru Akashi[4], Hajime Ohgushi[2] and Yoshiaki Yura[1]

[1]*Department of Oral and Maxillofacial Surgery, Graduate School of Dentistry, Osaka University, 1-8 Yamadaoka, Suita, Osaka, 565-0871, Japan*

[2]*Research Institute for Cell Engineering, National Institute of Advanced Industrial Science and Technology, Amagasaki Site, 3-11-46 Nakoji, Amagasaki, Hyogo, 661-0974, Japan*

[3]*Division of Materials and Manufacturing Science, Graduate School of Engineering, Osaka University, 2-1 Yamadaoka, Suita, Osaka, 565-0871, Japan*

[4]*Division of Applied Chemistry, Graduate School of Engineering, Osaka University, 2-1 Yamadaoka, Suita, Osaka, 565-0871, Japan*

Abstract

The authors previously created HAp or $CaCO_3$ formed on or in agarose gels (HAp and $CaCO_3$ gels, respectively) as biocompatible and biodegradable bone graft materials. However, these gels have limitations for bone regeneration. Mesenchymal stromal cells (MSCs) have osteogenic potential and are considered useful for bone tissue engineering. The purpose of this study was to clarify the osteogenic abilities of MSCs loaded in HAp or $CaCO_3$ gels (MSC/HAp and MSC/$CaCO_3$ gels, respectively) using a rat cranial defect model compared to HAp and $CaCO_3$ gels alone. HAp, $CaCO_3$, MSC/Hap, and MSC/$CaCO_3$ gels were prepared for *in vivo* analyses and implanted into full-thickness bone defects created in the rat cranium. All samples were assessed radiologically and histologically at 4 and 8 weeks after implantation. Using microfocus-computed tomography, an increase in bone formation was observed in the MSC-loaded gels compared to the gels alone. In addition, peripheral quantitative computed tomography revealed higher bone mineral contents in the MSC-loaded gels compared to the gels alone. After transmission X-ray diffraction analyses, the degree of apatite *c*-axis orientation as a bone quality index of newly formed bone in the MSC-loaded gels was close to that of living cranial bone. Histologically, more extensive bone formation was detected in the MSC-loaded gels compared to gels alone. Overall, MSC/HAp and MSC/$CaCO_3$ gels showed equivalent efficacy for bone regeneration. These findings demonstrate that loading of MSCs into the gels strengthened their osteogenic ability and improved the quality of the newly formed bone. As a result, MSC-loaded gels could represent viable therapeutic biomaterials for bone tissue engineering.

Received 28 October 2010; Revised 29 March 2011; Accepted 12 July 2011

Keywords hydroxyapatite; calcium carbonate; agarose gel; tissue engineering; mesenchymal stromal cell; bone regeneration; rat cranium; bone quality

1. Introduction

The various bone defects caused by tumour resection, treatment of infection, trauma, and congenital cleft jaw are challenging problems in the field s of orthopaedic, oral, and maxillofacial surgery. Bone grafting is a vital component of many surgical procedures that facilitate the repair of bony defects (Boyne *et al.*, 1980; Zhang *et al.*, 2010). Although autologous bone grafting is a popular procedure, it has many disadvantages such as limited supply of suitable bone, requirement of a second surgical site to harvest the bone, possible postoperative complications related to the harvesting procedure, and long surgical time. To overcome these difficulties, many types of biomaterials have been developed for bone regeneration.

* *Correspondence to: Koji Hattori, Research Institute for Cell Engineering, National Institute of Advanced Industrial Science and Technology, Amagasaki Site, 3-11-46 Nakoji, Amagasaki, Hyogo 661–0974, Japan. E-mail: koji-hattori@aist.go.jp*

Hydroxyapatite (HAp) is the main inorganic component of bone and teeth, and calcium carbonate ($CaCO_3$) is the main inorganic component of mollusc shells and pearls. HAp and $CaCO_3$ are well known to show good cell adhesion, proliferation, and differentiation properties (Hott *et al.*, 1997; Hanein *et al.*, 1993). Furthermore, they have shown bone-bonding properties (Okumura *et al.* 1991; Okumura *et al.*, 1997; Ohgushi *et al.*, 1992). Based on these excellent properties, sintered HAp and $CaCO_3$ ceramics have been used as bone graft substitutes. However, these ceramics are brittle and difficult to handle. To overcome their weak mechanical properties, HAp and $CaCO_3$ can be conjugated with organic polymers such as collagens and polysaccharides to obtain elastic properties. The current authors previously developed a novel alternate soaking process for preparing organic-inorganic complexes (Taguchi *et al.* 1998; Taguchi *et al.*, 1999a, 1999b). This process was based on the widely known wet process for HAp or $CaCO_3$ formation on organic polymer hydrogels by alternate soaking in solutions containing Ca^{2+} and PO_4^{3-} or CO_3^{2-} (Ogomi *et al.*, 2003). The current study selected agarose gel as an organic polymer hydrogel because it has several advantages as a substitute for biomineralization as follows (Watanabe *et al.*, 2007). 1) It is a physically crosslinked hydrogel that does not require a chemical catalyst; 2) It is a hydrolyzable compound at a low pH; 3) It is a nonimmunogenic compound unlike animal-derived substances; and 4) It is easy to prepare and handle. Based on previous experience, this study created novel biomaterials comprised of HAp or $CaCO_3$ formed on agarose gels (HAp and $CaCO_3$ gels, respectively) as biocompatible and biodegradable bone graft materials. By *in vitro* dissolution experiments, it has been reported that HAp gel is difficult to degrade at pH 7.4; however, both HAp and $CaCO_3$ gels showed rapid degradation capabilities after *in vivo* implantation (Watanabe *et al.*, 2007; Suzawa *et al.*, 2010). Concerning the mechanical properties, the current study showed that the average breaking stress and Young's modulus of HAp gel were much greater than those of $CaCO_3$ gel (Suzawa, 2010). These data demonstrate obvious differences between HAp and $CaCO_3$ gels.

The current study showed that both HAp and $CaCO_3$ gels allowed bone healing in a partial-thickness rat cranial defect model (Suzawa *et al.*, 2010). However, the gels did not show any healing potential for full-thickness cranial defects. As a result, these gels have limitations for bone regeneration. Tissue engineering approaches involving various cells, growth factors, and biocompatible scaffolds or combinations of these components have been shown to be very effective for bone regeneration (Langer *et al.*, 1993). It is widely accepted that MSCs existing in the bone marrow are multipotent cells that are capable of differentiating into osteoblasts, chondrocytes, adipocytes, and myoblasts (Owen *et al.*, 1988; Pittenger *et al.*, 1999). Since the osteogenic potential of MSCs has been confirmed by *in vitro* culture and *in vivo* implantation, MSCs are considered useful for bone tissue engineering (Ohgushi *et al.*, 1999; Ohgushi *et al.*, 2003).

The purpose of the current study was to clarify the osteogenic abilities of MSCs loaded into HAp or $CaCO_3$ gels (MSC/HAp and MSC/$CaCO_3$ gels, respectively) using a rat cranial defect model compared to those of the gels alone, and thereby to investigate their usefulness for tissue engineering approaches.

2. Materials and methods

2.1. Formation of HAp or $CaCO_3$ on or in agarose gels

The procedure for the formation of HAp or $CaCO_3$ on agarose gels has been previously described (Tabata *et al.*, 2003). Briefly, boiled aqueous solutions containing 3% (w/v) agarose (NuSieve; Cambrex Bio Science Rockland, Rockland, ME, USA) were poured into molds created at 0.5-mm intervals between two glass slides and then cooled. The resulting agarose gels of 0.5-mm thickness were punched out into discs of 4-mm diameter. The shaped gel discs were placed into the rat cranial bone defects. To prepare HAp gels, the gel discs were alternately soaked in aqueous solutions of $CaCl_2$ (pH 7.4, 200 mmol/l) and Na_2HPO_4 (120 mmol/l) at 4 °C for 2 h followed by washing in ultrapure water after each immersion. The soaking process in each ionic solution and washing was defined as one cycle and the process was repeated alternately for 12 cycles. $CaCO_3$ gels were prepared in a similar manner, except that the gel discs were soaked in Na_2CO_3 (200 mmol/l) solution instead of Na_2HPO_4 solution. The resulting HAp and $CaCO_3$ gels were finally immersed in ultrapure water and sterilized by 25 kGy gamma-ray irradiation (Koga Isotope, Shiga, Japan) for about 2 h before cell seeding. The agarose, Hap, and $CaCO_3$ gels were analyzed using a JSM-6700FE scanning electron microscopy (SEM) (JEOL, Tokyo, Japan) (Figure 1).

2.2. MSC preparation and loading in HAp/$CaCO_3$ gels

Rat MSCs were prepared according to previously reported methods (Ohgushi *et al.*, 1996a 1996a, 1996b). Briefly, bone marrow cells were obtained from the femoral bone shafts of 7-week-old Fischer 344 male rats purchased from Japan SLC (Shizuoka, Japan). Both ends of the femoral epiphyses were cut off and the bone marrow was flushed out using 10 ml of standard medium through a 21-gauge needle. The released bone marrow cells were seeded into T-75 flasks (BD Biosciences, Bedford, MA, USA) containing 15 ml of standard medium and cultured in a humidified atmosphere of 95% air and 5% CO_2 at 37 °C. One flask was used for the cells from each femoral shaft. The standard medium consisted of minimum essential medium (MEM) (Nacalai Tesque Inc., Kyoto, Japan) supplemented with 15% foetal bovine serum (JRH Bioscience, Lenexa, KS, USA) and 1% antibiotics (100 U/ml penicillin, 100 μg/ml streptomycin, 0.25 μg/ml

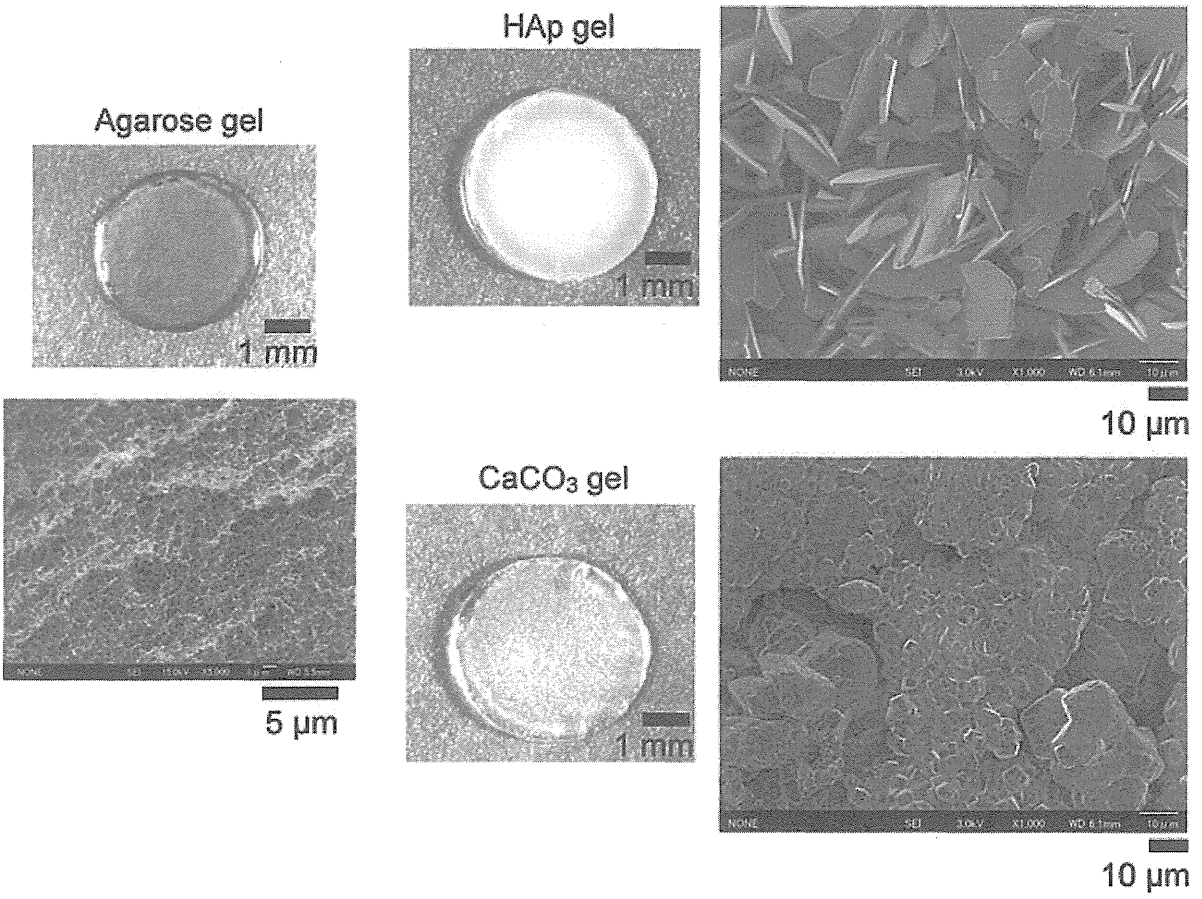

Figure 1. Macroscopic and SEM images of agarose, Hap, and $CaCO_3$ gels. The gel disks were implanted in rat full-thickness cranial defects. Crystals of HAp and $CaCO_3$ particles were observed with various sizes of diameter from about several nm to a few μM by SEM analyses

amphotericin B) (Sigma-Aldrich, St. Louis, MO, USA). To remove non-adherent cells, the medium was renewed three times per week. The cell culture was maintained for about 7 days until the cells reached confluence. It was reported that the prepared adherent cells were mesenchymal type cells with differentiation capabilities towards osteoblasts (Ohgushi *et al.*, 1996a, 1996b; Tanaka *et al.*, 2009; Kato *et al.*, 2011), vascular endothelial cells (Nagaya *et al.*, 2005), and hepatocytes (Oyagi *et al.*, 2006). The adherent cells were therefore considered as MSCs and thereby detached from the flasks using 0.05% trypsin, harvested, and resuspended in culture medium at a density of 1 x 10^7 cells/ml. Next, 1-ml aliquots of the cell suspension were applied to the disk-shaped HAp and $CaCO_3$ gels in 15-mm tissue culture plates and the mixtures were left to stand overnight in a humidified atmosphere of 95% air and 5% CO_2 at 37 °C. For preparation of the 1 x 10^7 cells, the cells were harvested from three T-75 flasks. The resulting MSC-loaded HAp and $CaCO_3$ gels (MSC/HAp and MSC/$CaCO_3$ gels, respectively) were implanted into the rat cranial defects.

2.3. Implantation

Fischer 344 male rats (8-weeks-old) were anesthetized by an intraperitoneal injection of sodium pentobarbital (Nembutal; Dainippon Pharmaceutical, Tokyo, Japan) at a final concentration of 40 mg/kg body weight. After shaving the skin, a midline incision was made in the skull and the periosteum was opened to expose the surface of the parietal bones. A 4-mm diameter full-thickness round cranial defect was created bilaterally in the parietal bone using a trephine bur (Trephine Drill; Storz am Mark Gmbh, Emmingen-Liptingen, Germany) with minimum saline irrigation. Each defect was rinsed with saline to remove any remaining debris and then implanted with the experimental gels (Figure. 2). The defects on the right side were implanted with MSC/HAp or MSC/$CaCO_3$ gels ($n = 6$). The defects on the left side were implanted with HAp or $CaCO_3$ gels without MSCs ($n = 6$ h). As controls, other cranial defects were washed with saline and left without any implants ($n = 6$). After implantation, the periosteum and skin were closed in layers with thread sutures.

The rats were returned to their cages and allowed to move freely. At 4 and 8 weeks after implantation, the rats were humanely terminated with an overdose of sodium pentobarbital and cranial bone samples were taken for the following analyses.

2.4. Microfocus-computed tomography (μ-CT)

A μ-CT imaging system for the analysis of small animals (SMX-100CT; Shimadzu, Kyoto, Japan) was used for the detection of newly formed bone in the cranial defects. The

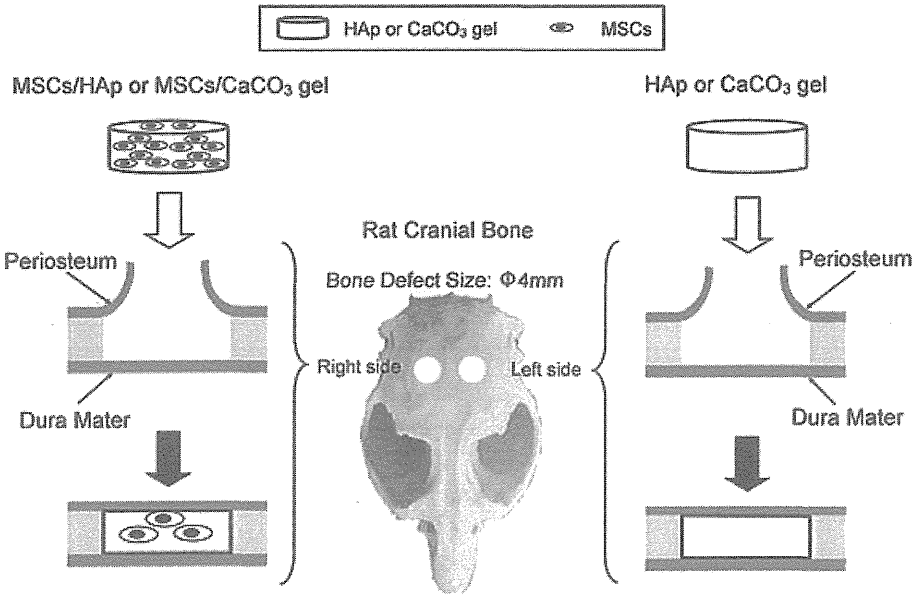

Figure 2. Schematic illustration of the rat cranial bone defect model. Full-thickness circular bone defects were produced in the rat cranial bone. The defects on the right side were implanted with MSC/HAp or MSC/$CaCO_3$ gels ($n = 6$). The defects on the left side were implanted with HAp or $CaCO_3$ gels without MSCs ($n = 6$). (MSCs, mesenchymal stromal cells; HAp gel, hydroxyapatite formed on agarose gel; $CaCO_3$ gel, calcium carbonate formed on/in agarose gel; MSC/HAp gel, MSC-loaded HAp gel; MSC/$CaCO_3$ gel, MSC-loaded $CaCO_3$ gel)

samples were scanned using a resolution of 42 μM and the isotropic voxel size was 600 views/180 degrees. The scanner was set at a voltage of 40 kV and a current of 33 μA. The sliced images were compiled and analyzed to render 3D images. Visual analyses of the μ-CT data were performed using the provided VGStudio software (Shimadzu).

2.5. Peripheral quantitative computed tomography (pQCT)

A pQCT system (XCT Research SA+, MDL922011; Stratec Medizintechnik, Pforzheim, Germany) was used to measure the volumetric bone mineral density (mg/cm^3) at arbitrary sites. Each sample was set in the gantry of the pQCT system and scanned with a 70-μM voxel size. Five serial cross-sectional slices (0.46-mm thickness) were scanned, of which the middle cross-section surface passed through the centre of the bone defect in the CT image. The scanning volume was a solid rectangle with a base of 3.96 x 1.15 mm and a height of 0.46 mm. A threshold of 267 mg/cm^3 was used to separate the newly formed bone from the surrounding tissues. The newly formed bone volume in the solid rectangle was set as the region of interest (ROI) using the ROI tool function, and the bone mineral density of the newly formed bone was determined. The bone mineral content (newly formed bone volume cm^3 x bone mineral density mg/cm^3) was used as a quantitative index in the pQCT assessment.

2.6. Microbeam X-ray diffraction (μ-XRD)

A μ-XRD system (R-AXIS BQ; Rigaku, Osaka, Japan) was used to analyze the preferential alignment of the *c*-axis of the biological apatite crystallites in the samples (Sasaki *et al.*, 2008). Molybdenum (Mo)-Kα radiation was generated at a tube voltage of 50 kV and a tube current of 90 mA, and the incident beam was focused onto a beam spot of 800 μM in diameter by a collimator. The beam was vertically directed against the surface of the newly formed bone that existed in each defect. Using the diffraction profile measured in an anteroposterior direction of the skull, the intensities of the (002) and (310) peaks were detected, and the integral intensity ratio (002/310) was calculated. Nakano *et al.* (2002) reported that the preferential alignment of the *c*-axis of biological apatite crystallites is strongly dependent on bone sections such as long bone, flat bone, or dentulous mandible, and can be assessed by the relative intensities between the (002) and (310) diffraction peaks. An increase in the relative intensity ratio indicated more frequent alignment of the *c*-axis of the biological crystallites.

2.7. Histological and histomorphometric analyses

The samples were fixed in 10% neutral-buffered formalin, decalcified with K-CX solution (Falma, Tokyo, Japan), and embedded in paraffin. Sagittal sections (4-μm thick) were prepared from the centre of the defects and stained with hematoxylin and eosin. For histomorphometric analysis, the newly formed bone areas in the defects were measured using Image-Pro® Plus J image software (Media Cybernetics, Bethesda, MD, USA). The bone area ratio (area of newly formed bone/area of cranial defect in the histological section) was used as a quantitative index in the histomorphometric assessment.

2.8. Statistical analysis

For comparisons between HAp or $CaCO_3$ gels alone and MSC/HAp or MSC/$CaCO_3$ gels, the differences were analyzed by the nonparametric Mann-Whitney U test. The significance level was set at $P < 0.05$.

3. Results

3.1. μ-CT findings

At 4 weeks after implantation, the radioopaque areas were larger in the MSC/HAp gels than in the HAp gels alone. Similarly, the radioopaque areas were larger in the MSC/$CaCO_3$ gels than in the $CaCO_3$ gels alone. At 8 weeks after implantation, the same tendencies were observed and the MSC-loaded gels contained larger radioopaque areas than the gels without MSCs. The radio-opacities of the MSC/HAp and MSC/$CaCO_3$ gels at 8 weeks after implantation were higher than those at 4 weeks after implantation. In defects without any implants, almost all areas were radiolucent at both 4 and 8 weeks after implantation (Figure 3, Defect).

3.2. pQCT findings

Figure 4 shows the data obtained in the pQCT analyses. At 4 weeks after implantation, the mean bone mineral contents were 824 mg in MSC/HAp gels, 284 mg in HAp gels, 918 mg in MSC/$CaCO_3$ gels, 411 mg in $CaCO_3$ gels, and 119 mg in defects without gels (Defect). Significant differences were found between MSC/HAp and HAp gels and between MSC/$CaCO_3$ and $CaCO_3$ gels. At 8 weeks after implantation, the mean bone mineral contents were 1019 mg in MSC/HAp gels, 464 mg in HAp gels, 1150 mg in MSC/$CaCO_3$ gels, 500 mg in $CaCO_3$ gels, and 192 mg in defects without gels (Defect). Significant differences were observed between MSC/HAp and HAp gels and between MSC/$CaCO_3$ and $CaCO_3$ gels.

3.3. μ- XRD findings

Figure 5 shows the integral intensity ratios of (002/310) corresponding to the degrees of preferential *c*-axis alignment in the newly formed bone. At 4 weeks after implantation, the mean integral intensity ratios of (002/310) were 1.5 in MSC/HAp gels, 0.35 in HAp gels, 1.45 in MSC/$CaCO_3$ gels, and 0.39 in $CaCO_3$ gels. Significant differences were found between MSC/HAp and HAp gels and between MSC/$CaCO_3$ and $CaCO_3$ gels. At 8 weeks after implantation, the mean integral intensity ratios of (002/310) were 1.9 in MSC/HAp gels, 0.52 in HAp gels, 1.7 in MSC/$CaCO_3$ gels, and 0.55 in $CaCO_3$ gels. Significant differences were found between MSC/HAp and HAp gels and between MSC/$CaCO_3$ and $CaCO_3$ gels.

3.4. Histological and histomorphometric findings

Histological and histomorphometric findings are shown in Figures 6 and 7, respectively. At 4 weeks after

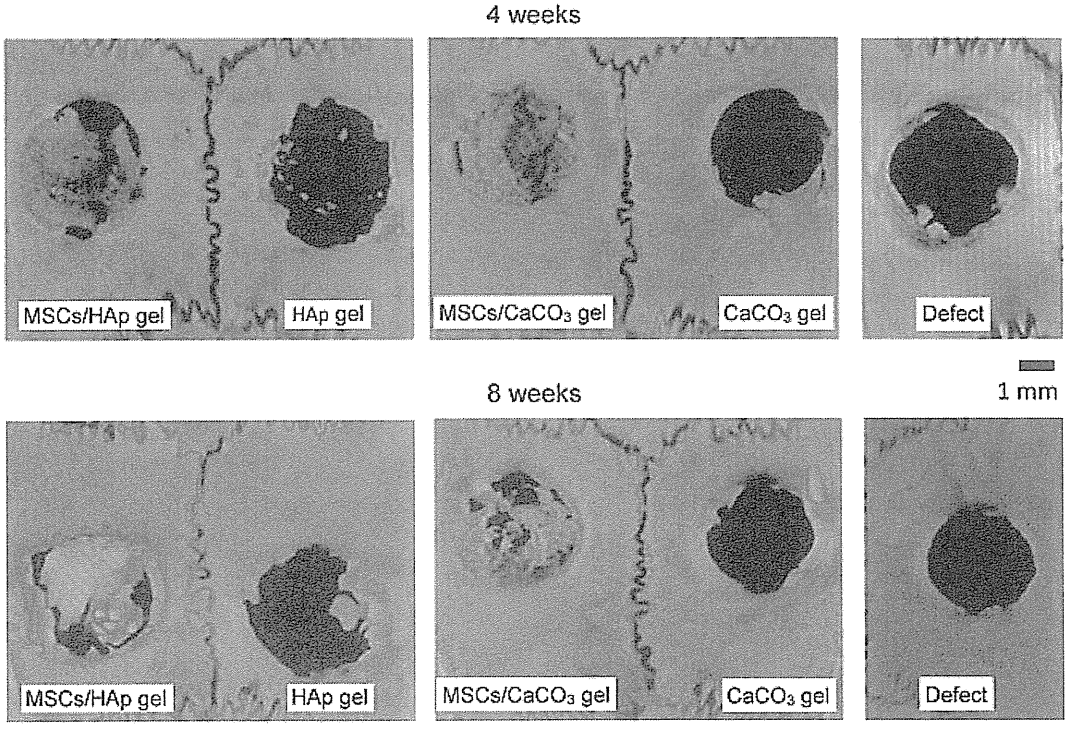

Figure 3. μ-CT images of rat calvariae. Upper panels: images at 4 weeks after implantation; lower panels: images at 8 weeks after implantation. Defect: cranial defects without any implants

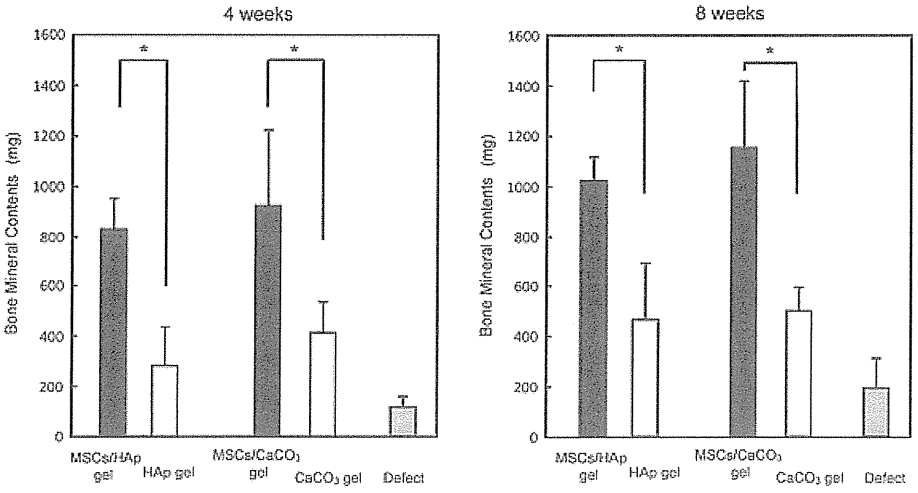

Figure 4. Bone mineral contents in MSC/HAp, HAp, MSC/$CaCO_3$, and $CaCO_3$ gels. The data are means + SD ($n = 6$). *$P < 0.05$

implantation, defect areas were covered with newly formed bone in MSC/HAp and MSC/$CaCO_3$ gels and the thickness of the newly formed bone in the defects were smaller than the pre-existing cranial bone. The defect areas in the HAp and $CaCO_3$ gels were filled with newly formed bone and fibrous tissues, but the bone areas were small compared with those in the defects in the MSC/HAp and MSC/$CaCO_3$ gels (Figures 6A-D). In contrast, control defects without any implants showed fibrous tissue without noticeable bone tissue (Figure. 6E). The mean bone area ratios were 0.57 in MSC/HAp gels, 0.22 in HAp gels, 0.59 in MSC/$CaCO_3$ gels, and 0.23 in $CaCO_3$ gels. Significant differences were found between MSC/HAp and HAp gels and between MSC/$CaCO_3$ and $CaCO_3$ gels (Figure. 7). At 8 weeks after implantation, the defect areas were covered with newly formed bone in the MSC/HAp and MSC/$CaCO_3$ gels, and the thickness of the newly formed bone were almost the same as the pre-existing cranial bone. The defect areas in the HAp and $CaCO_3$ gels were partly covered with newly formed bone but the newly formed bone was discontinuous and thinner than the pre-existing cranial bone (Figures 6F-6I). The newly formed bone was difficult to detect in the control defects (Figure. 6J). The mean bone area ratios were 0.68 in MSC/HAp gels, 0.30 in HAp gels, 0.70 in MSC/$CaCO_3$ gels, and 0.30 in $CaCO_3$ gels. Significant differences were found between MSC/HAp and HAp gels and between MSC/$CaCO_3$ and $CaCO_3$ gels (Figure. 7).

4. Discussion

Bone tissue is an organic-inorganic complex that consists of biomineral crystals such as HAp and type I collagen matrix. Various methods have been developed to create organic-inorganic complex materials that mimic bone tissue structure (Boskey, 1989; Kato *et al.*, 1996; Dalas *et al.*, 2000; Kokubo, 1990; Yamamoto *et al.*, 1998; Kato *et al.*, 1998; Kato *et al.*, 2000). Most of these methods require a long period of time to deposit large amounts of biomineral

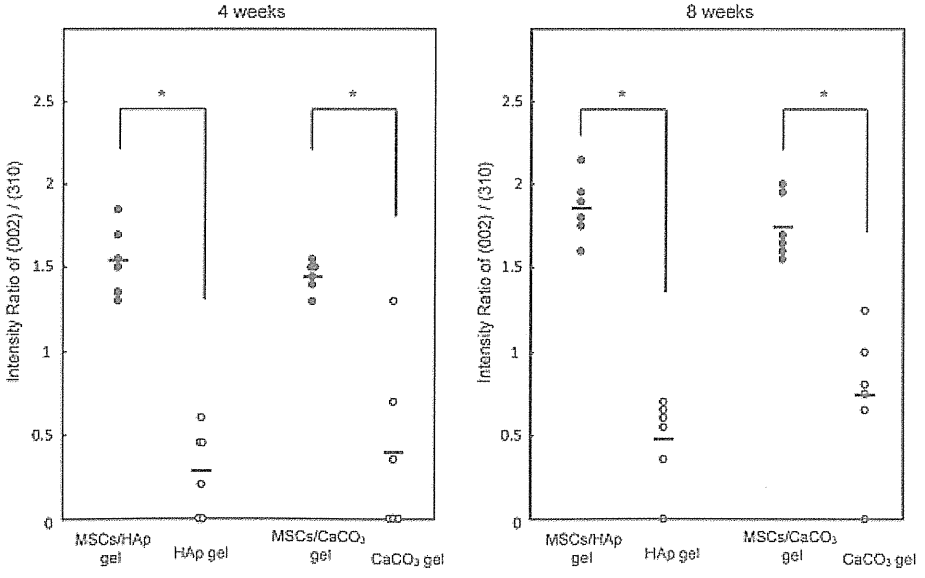

Figure 5. Intensity ratios of (002/310) of MSC/HAp, HAp, MSC/$CaCO_3$, and $CaCO_3$ gels. *$P < 0.05$

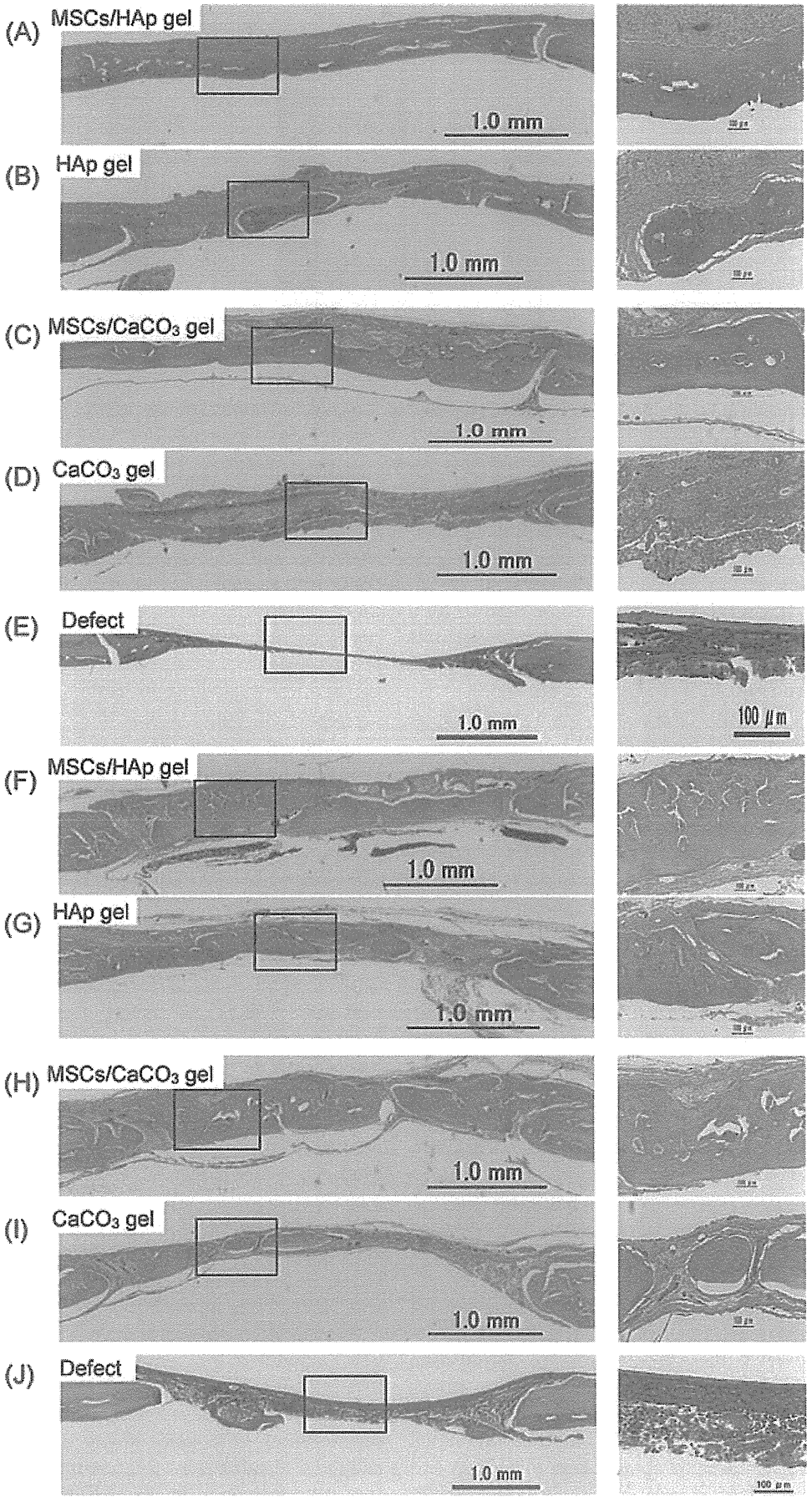

Figure 6. Histology of rat cranial defects implanted with MSC/HAp, HAp, MSC/$CaCO_3$ $CaCO_3$ gels, and control defect without any implants. A-E) Histology at 4 weeks after implantation. F-J) Histology at 8 weeks after implantation. The right panels show magnified images of the rectangles in the left panels

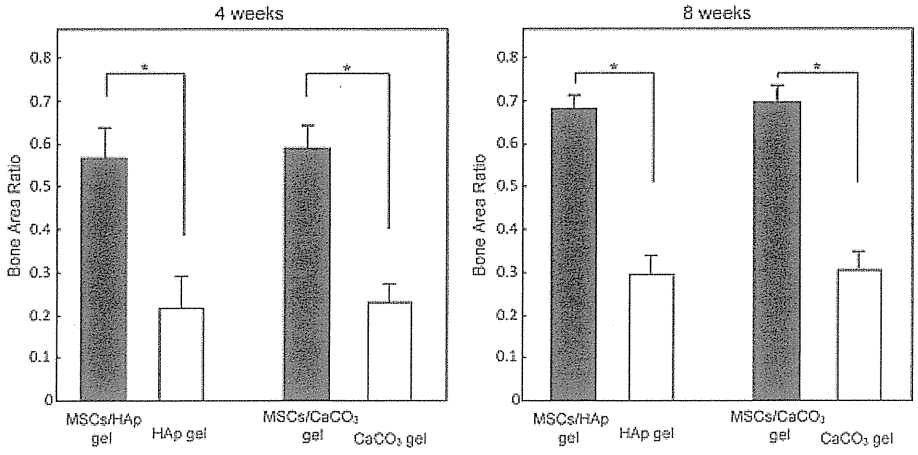

Figure 7. Bone area ratios in the MSC/HAp, HAp, MSC/$CaCO_3$, and $CaCO_3$ gels. The data are means + SD ($n = 6$). * $P < 0.05$

on organic materials. An alternate soaking process that was previously developed formed HAp on biomaterials approximately 100x faster than conventional biomimetic processes (Taguchi *et al.*, 1998; Taguchi *et al.*, 1999a, 1999b; Tachaboonyakiat *et al.*, 2001; Tachaboonyakiat *et al.*, 2002). Moreover, this process could also be used to form $CaCO_3$ on materials (Ogomi *et al.*, 2003) and the amounts of HAp or $CaCO_3$ could be easily controlled by the reaction conditions (Taguchi *et al.*, 2001; Ogomi *et al.*, 2005).

In addition to HAp, $CaCO_3$ also exhibits excellent compatibility with hard tissues (Guillemin *et al.*, 1987; Ohgushi *et al.*, 1992). In the current study, the osteogenic abilities of MSC/HAp and MSC/$CaCO_3$ gels were assessed and both types of gels showed equivalent efficacy for bone regeneration in a rat cranial defect model. Although $CaCO_3$ gels are inferior to HAp gels in terms of their mechanical strength, the biodegradation of $CaCO_3$ is faster than that of HAp (Ohgushi *et al.*, 1992). As a result, HAp or $CaCO_3$ gels can be selected depending on the clinical situation.

The usefulness of HAp or $CaCO_3$ gels for hard tissue regeneration has been assessed using several animal models. Tabata *et al.* (2005) assessed HAp gels as bone-grafting materials for the treatment of surgically created, chronic periodontal defects in dogs. At 6 months after implantation, newly formed bone was significantly observed. They also reported on the haemostatic properties of HAp gels when used as fillers for tooth-extraction sockets in adult monkeys (Tabata *et al.*, 2003). Moreover, osteogenic behaviour of $CaCO_3$ gels as well as HAp gels have also been observed in bone defects in the rat cranium (Suzawa *et al.*, 2010). These observations demonstrate the excellent osteogenic properties of HAp and $CaCO_3$ gels in bone defect models. However, these models involved partial bone defects rather than full-thickness defects. As a result, in the current study, the gels were loaded with MSCs to evaluate their bone regeneration abilities in rat cranial full-thickness defects. Results showed that MSC/HAp and MSC/$CaCO_3$ gels exhibited greater bone-forming capabilities than HAp and $CaCO_3$ gels without MSCs.

The *c*-axis of biological apatite crystallites is distributed along the extending collagen fibrils in calcified tissues such as bone and teeth, and the combination of biological apatite with collagen fibrils as well as the microstructure of these substances are known to affect the mechanical, chemical, and biological properties (Landis, 1995). As a result, the current study examined the preferential alignment of the *c*-axis of biological apatite crystallites in the newly formed bone in the cranial defects. A μ-XRD system is a powerful tool for analyzing the orientation of biological apatite crystallites in bone (Nakano *et al.*, 2002; Nakano *et al.*, 2007). Ishimoto *et al.* (2010) showed that the intensity ratios of (002/310) in intact rat parietal bone ranged from 1.0-3.0. In the current study, the intensity ratios of the newly formed bone were 1.5 in MSC/HAp gels, 0.35 in HAp gels, 1.45 in MSC/$CaCO_3$ gels, and 0.39 in $CaCO_3$ gels. As a result, the newly formed bone in both MSC/HAp and MSC/$CaCO_3$ gels was more mature than that in HAp and $CaCO_3$ gels.

Concerning the role of MSCs for additive osteogenic responses, it has already been reported that implantation of MSCs at rat cranial defects (Tanaka *et al.*, 2009) or femoral bone defects (Nakamura *et al.*, 2010) showed new bone in which signals of donor MSCs were detected. It has also been reported that rat (Nagaya *et al.*, 2005) and human (Kagiwada *et al.*, 2008) MSCs produce large quantities of angiogenic factors such as vascular endothelial growth factor (VEGF) during *in vitro* culture as well as after *in vivo* implantation. VEGF is known to enhance osteogenesis and as a result, donor cells of MSC/HAp and MSC/$CaCO_3$ at the rat cranial full-thickness defects could survive and differentiate into bone forming osteoblasts. Furthermore, the MSCs themselves showed trophic effects feasible for bone formation.

In conclusion, this study revealed that HAp and $CaCO_3$ gels loaded with MSCs have excellent osteogenic abilities in a rat full-thickness cranial defect model and that both HAp and $CaCO_3$ gels are suitable scaffolds for bone tissue regeneration. Osteogenic ability was assessed radiologically and histologically. μ-CT results showed more extensive bone formation in the MSC-loaded gels than in the gels alone. Moreover, pQCT analyses revealed that the bone mineral contents were higher in the MSC-loaded gels than in the gels alone. μ-XRD analyses showed that

the crystallographic microstructures of the newly formed bone in the MSC-loaded gels were close to that of living cranial bone. Histologically, more extensive bone formation was detected in the MSC-loaded gels than in the gels alone. These findings show that loading of MSCs into the gels strengthened their osteogenic ability and improved the quality of the newly formed bone. As a result, MSC/HAp and MSC/$CaCO_3$ gels can be used as therapeutic biomaterials in bone tissue engineering.

Acknowledgments

The authors wish to thank their many colleagues for their support during this study, especially Dr. Takuya Ishimoto, Graduate School of Engineering, Osaka University for providing expertise and support in the radiological analyses. This study was supported in part by Grants-in-Aid from the Ministry of Education, Culture, Sports, Science and Technology of Japan. The study sponsors had no role in the study design, data analysis, or data interpretation, or in the writing of the report.

References

Boskey AL. 1989; Hydroxyapatite formation in a dynamic collagen gel system. Effect of type I collagen, lipids, and proteoglycans. *J Phys Chem* **93**: 1628–1633.

Boyne PJ, James RA. 1980; Grafting of the maxillary sinus floor with autogenous marrow and bone. *J Oral Surg* **38**: 613–616.

Dalas E, Klepetsanis PG, Koutsoukos PG. 2000; Calcium carbonate deposition on cellulose. *J Colloid Interface Sci* **224**: 56–62.

Guillemin G, Patat JL, Fournie J *et al.* 1987; The use of coral as a bone graft substitute. *J Biomed Mater Res* **21**: 557–567.

Hanein D, Sabanay H, Addadi L *et al.* 1993; Selective interactions of cells with crystal surface: Implications for the mechanism cell adhesion. *J Cell Sci* **104**: 275–288.

Hott M, Noel B, Bernache-Assolant D *et al.* 1997; Proliferation and differentiation of human trabecular osteoblastic cells on hydroxyapatite. *J Biomed Mater Res* **37**: 508–516.

Ishimoto T, Sakamoto T, Nakano T. 2010; Orientation of biological apatite in rat calvaria analyzed by microbeam X-ray diffractmeter. *Mater Sci Forum* **638–642**: 576–581.

Kagiwada H, Yashiki T, Ohshima A *et al.* 2008; Human mesenchymal stem cells as a stable source of VEGF-producing cells. *J Tissue Eng Regen Med* **2**: 184–189.

Kato K, Eika Y, Ikada Y. 1996; Deposition of hydroxyapatite thin layer onto a polymer surface carrying grafted phosphate polymer chain. *J Biomed Mater Res* **32**: 687–691.

Kato T, Hattori K, Deguchi T *et al.* 2011; Osteogenic potential of rat stromal cells derived from periodontal ligament. *J Tissue Eng Regen Med* **5**: 798–805.

Kato T, Suzuki T, Amamiya T *et al.* 1998; Effect of macromolecules on the crystallization of $CaCO_3$ the formation of organic/inorganic composite. *Supramol Sci* **5**: 411–415.

Kato T, Suzuki T, Irie T. 2000; Layered thin-film composite consisting polymer and calcium carbonate: A novel organic/inorganic material with organized structure. *Chem Lett* **29**: 186–187.

Kokubo T. 1990; Surface chemistry of bioactive glass-ceramics. *J Non-Cryst Sol* **120**: 138–151.

Landis WJ. 1995; The strength of a calcified tissue depends in part on the molecular structure and organization of its constituent mineral crystals in their organic matrix. *Bone* **16**: 533–44.

Langer R, Vacanti JP. 1993; Tissue engineering. *Science* **260**: 920–926.

Mingyu Zhang, Kunzheng Wang, Zhibin Shi *et al.* 2010; Osteogenesis of the construct combined BMSCs with b-TCP in rat. *J Plast Reconstr Aesthet Surg* **63**(2): 227–232.

Nagaya N, Kangawa K, Itoh T *et al.* 2005; Transplantation of mesenchymal stem cells improves cardiac function in a rat model of dilated cardiomyopathy. *Circulation* **112**: 1128–1135.

Nakamura A, Akahane M, Shigematsu H *et al.* 2010: Cell sheet transplantation of cultured mesenchymal stem cells enhances bone formation in a rat nonunion model. *Bone* **46**: 418–424.

Nakano T, Ishimoto T, Umakoshi Y *et al.* 2007; Variation in bone quality during regenerative process. *Mater Sci Forum* **539–543**: 675–680.

Nakano T, Kaibara K, Tabata Y *et al.* 2002; Unique alignment and texture of biological apatite crystallites in typical calcified tissues analyzed by microbeam X-ray diffractometer system. *Bone* **31**: 479–487.

Ogomi D, Serizawa T, Akashi M. 2003; Bioinspired organic–inorganic composite materials prepared by an alternate soaking process as a tissue reconstitution matrix. *J Biomed Mater Res* **67A**: 1360–1366.

Ogomi D, Serizawa T, Akashi M. 2005; Controlled release based on the dissolution of a calcium carbonate layer deposited on hydrogels. *J Control Release* **103**: 315–323.

Ohgushi H, Caplan AI. 1999; Stem cell technology and bioceramics: from cell to gene engineering. *J Biomed Mater Res* **48**: 913–927.

Ohgushi H, Dohi Y, Katuda T *et al.* 1996a; In vitro bone formation by rat marrow cell culture. *J Biomed Mater Res* **32**: 333–340.

Ohgushi H, Dohi Y, Yoshikawa T *et al.* 1996b; Osteogenic differentiation of cultured marrow stromal stem cells on the surface of bioactive glass ceramics. *J Biomed Mater Res* **32**: 341–348.

Ohgushi H, Miyake J, Tateishi T. 2003; Mesenchymal stem cells and bioceramics: strategies to regenerate the skeleton. *Novartis Found Symp* **249**: 118–127.

Ohgushi H, Okamura M, Yoshikawa T *et al.* 1992; Bone formation process in porous calcium carbonate and hydroxyapatite. *J Biomed Mater Res* **26**: 885–895.

Okumura M, Ohgushi H, Tamai S. 1991; Bonding osteogenesis in coralline hydroxyapatite combined with bone marrow cells. *Biomaterials* **12**: 411–416.

Okumura M, Ohgushi H, Dohi Y *et al.* 1997; Osteoblastic phenotype expression on the surface of hydroxyapatite ceramics. *J Biomed Mater Res* **37**: 122–129.

Owen M, Friedenstein AJ. 1988; Stromal stem cells: marrow derived osteogenic precursors. *Ciba Found Symp* **136**: 42–60.

Oyagi S, Hirose M, Kojima M, Okuyama M *et al.* 2006; Therapeutic effect of transplanting HGF-treated bone marrow mesenchymal cells into CCl4-injured rats. *J Hepatol* **44**: 742–748.

Pittenger MF, Mackay AM, Beck SC *et al.* 1999; Multilineage potential of adult human mesenchymal stem cells. *Science* **284**: 143–147.

Sasaki K, Nakano T, Ferrara JD *et al.* 2008; New technique for evaluation of preferential alignment of biological apatite (BAp) crystallites in bone using transmission X-ray diffractometry. *Mater Trans* **49**: 2129–2135.

Suzawa Y. 2010; Assessment of biomineral/agarose composite as a scaffold for bone tissue engineering. *Graduate school of Dentistry, Osaka University, Thesis.*

Suzawa Y, Funaki T, Watanabe J *et al.* 2010; Regenerative behavior of biomineral/agarose composite gels as bone grafting materials in rat cranial defects. *J Biomed Mater Res A* **93**: 965–975.

Tabata M, Shimoda T, Sugihara K *et al.* 2005; Apatite formed on/in agarose gel as a bone-grafting material in the treatment of periodontal infrabony defect. *J Biomed Mater Res B Appl Biomater* **75**: 378–386.

Tabata M, Shimoda T, Sugihara K *et al.* 2003; Osteoconductive and hemostatic properties of apatite formed on/in agarose gel as a bone-grafting material. *J Biomed Mater Res B Appl Biomater* **67**: 680–688.

Tachaboonyakiat W, Serizawa T, Akashi M. 2001; Hydroxyapatite formation on/in biodegradable chitosan hydrogels by an alternate soaking process. *Polym J* **33**: 177–181.

Tachaboonyakiat W, Serizawa T, Akashi M. 2002; Inorganic-organic polymer hybrid scaffold for tissue engineering II: Partial enzymatic degradation of hydroxyapatite-chitosan hybrid. *J Biomed Polym Ed* **13**: 1021–1032.

Taguchi T, Kishida A, Akashi M. 1998; Hydroxyapatite formation on/in hydrogels using a novel alternate soaking process. *Chem Lett* **27**: 711–712.

Taguchi T, Kishida A, Akashi M. 1999a; Apatite formation on/in hydrogel matrices using an alternate soaking process. II Effect of swelling ratios of poly (vinyl alcohol) hydrogel matrices on apatite formation. *J Biomater Sci Polymer Ed* **10**: 331–339.

Taguchi T, Kishida A, Akashi M. 1999b; Apatite formation on/in hydrogel matrices using an alternate soaking process. III Effect of physico-chemical factor on apatite

formation on/in poly(vinyl alcohol) hydrogel matrices. *J Biomater Sci Polymer Ed* **10**: 795–804.
Taguchi T, Kishida A, Akashi M. 2001; Apatite coating on hydrophilic polymer-grafted poly (ethylene) films using an alternate soaking process. *Biomaterials* **22**: 53–58.
Tanaka T, Hirose M, Kotobuki N *et al.* 2009; Bone augmentation by bone marrow mesenchymal stem cells cultured in three-dimensional biodegradable polymer scaffolds. *J Biomed Mater Res A* **91**: 428–435.
Watanabe J, Kashii M, Hirao M *et al.* 2007; Quickly-forming hydroxyapatite/agarose gel composites induce bone regeneration. *J Biomed Mater Res A* **83A**: 845–852.
Yamamoto S, Miyamot T, Kokubo T *et al.* 1998; Preparation of polymer-silicate hybrid materials bearing silanol groups and the apatite formation on/in the hybrid materials. *Polym Bull* **40**: 243-/250.